Fluid-driven Cyclic Reorganisation in Shallow Basaltic Fault Zones

Bob Bamberg[1], Richard Walker[1,2], Marc Reichow[1], Audrey Ougier-Simonin[3]

[1]School of Geography, Geology, and the Environment, University of Leicester, University Road, Leicester LE1 7RH, United Kingdom

[2]Department of Earth and Planetary Sciences, University of California, Davis, 1 Shields Avenue, Davis, CA 95616, US

[3]Rock Mechanics and Physics Laboratory, British Geological Survey, Nicker Hill, Keyworth, Nottingham NG21 5GG, United Kingdom

Contact Details

B. Bamberg: bobbamberg@gmail.com (corresponding author)
R. Walker: rjwalker@ucdavis.edu
M. Reichow: mkr6@le.ac.uk
A. Ougier-Simonin: audreyo@bgs.ac.uk

Keywords

Fault evolution, basalt, fluid flow, cementation, weakening, alteration

This preprint has been accepted for publication in **Geosphere** but does not include final copyediting and typesetting changes. Once the published version is available, it can be accessed via a link on the article webpage.

Fluid-Driven Cyclic Reorganisation in Shallow Basaltic Fault Zones

Bob Bamberg, Richard Walker, Marc Reichow, Audrey Ougier-Simonin

Abstract

Faults represent a critical heterogeneity in basaltic sequences, yet few studies have focused on their architectural and hydromechanical evolution. We present a detailed multi-scale characterisation of passively exhumed fault zones from the layered basalts of the Faroe Islands, which reveals cyclic stages of fault evolution. Outcrop-scale structures and fault rock distribution within the fault zones were mapped in the field and in 3D virtual outcrop models, with detailed characterisation of fault rock microstructure obtained from optical and scanning electron microscopy. The fault zones record deformation localisation from decametre-wide Riedel shear zones into metre-wide fault cores, containing multiple cataclastic shear bands and low strain lenses organised around a central slip zone. Shear bands and the slip zone consist of (ultra-) cataclasites with a zeolite-smectite assemblage replacing the original plagioclase-pyroxene host rock composition. Low-strain lenses are breccias of weakly altered host rock, or reworked fault rocks. Slip zone-proximal zones show significant late-stage dilatation in the form of hydrothermal breccias or tabular veins with up to decimetre apertures. We interpret these structures as evolving from alternating shear-compaction and dilation through hydrofracture. The fault core preserves slip zone reworking, which is interpreted to indicate repeated shear zone locking and migration. The alternating deformation styles of shear-compaction and dilatation suggest episodic changes in deformation mechanisms driven by transient overpressure and release. The fault zone mechanical properties are thus governed by the combined effects of permanent chemical weakening and transient fluid-mediated mechanical weakening, alternating with cementation and healing. We suggest that the model presented for fault evolution should apply widely to shallow basalt-hosted fault zones.

1 Introduction

Faults represent a critical heterogeneity in basaltic sequences, yet few studies have detailed their architectural and hydromechanical evolution. Much work has been dedicated to understanding the evolution of the surface-expression of fault zones in basalts, with the main focus on fissure-type surface breaching faults (e.g. Holland et al., 2006; Bubeck et al., 2018; Von Hagke et al., 2019), and/or on fault growth in units with a strong mechanical anisotropy such as cooling joints (e.g. Walker et al., 2012; Soden and Shipton, 2013; Crider, 2015; Kettermann et al., 2019; Weismüller et al., 2019). Relatively few studies have focused on the internal architecture and evolution of fault rock development in basaltic systems at depth. In the subsurface, basalts undergo pervasive fluid-mediated alteration during fault evolution (Kristmannsdóttir, 1979; Walker et al., 2013a), with the new mineral assemblage drastically changing bulk-rock mechanical properties, such as replacement of frictionally strong feldspar-dominated assemblages by relatively weak zeolites (Yukselen-Aksoy, 2010; Frolova et al., 2014) or clay minerals (Shimamoto and Logan, 1981; Haines et al., 2013; Boulton et al., 2014; Carpenter et al., 2016). These mineralogic changes not only affect the mechanical structure, but also the permeability structure of the fault (Walker et al., 2013a; Walker et al., 2013b), which may also affect fault strength and stability.

Although some studies have characterised the evolution and deformation mechanisms operating at small displacement scales for faults in basalts (millimetre- to decametre-scale displacement: Walker et al., 2012; 2013a; 2013b), and performed initial description of fault displacement versus fault damage thickness scaling, these studies have not performed detailed analysis of the deformation mechanisms responsible for slip zone and fault zone growth at larger displacement scales, nor the processes that may lead to fault core thickening.

In this study, we seek to characterise the relationship between fluids and fault zone evolution in basaltic rocks based on exceptionally well-exposed field sites in the Faroe Islands, on the NE Atlantic margin. We focus on three exhumed large-displacement (decametre- to potentially kilometre-scale) fault zones, that were active at ca. 1–2 km depth (Figure 1). We studied fault architecture in the field and in virtual outcrop models acquired using Unoccupied Airborne Vehicle (UAV)-derived photogrammetric models, and microstructures were observed using petrographic microscopes and Scanning Electron Microscope – Backscattered Electron (SEM-BSE) imaging. Mineral identification is based on X-Ray Diffraction (XRD) and Scanning Electron Microscope – Energy Dispersive Spectroscopy (SEM-EDS) in combination (data in the digital supplement) with petrographic microscopy. From these observations, we identify deformation mechanisms within a framework of cyclic fault zone evolution, involving cataclastic deformation punctuated by episodic hydrofracture restrengthening, and slip zone migration. Our results and conceptual model may have implications for, and application to, the mechanical and permeability evolution in large-displacement faults in basaltic rocks more broadly.

2 Background

2.1 Fault Evolution

Fault zones that have accommodated multiple slip events typically display a complex internal architecture, featuring weakly deformed fault rock lenses hosted in anastomosing cataclastic shear bands (Faulkner et al., 2003). This anastomosing macrostructure can arise from shear zone locking and slip migration as a consequence of strain- or mineralisation-hardening (Faulkner et al., 2003; Caine et al., 2010; Callahan et al., 2020). Other faults show evidence for periodic roughening through slip zone segmentation, followed by progressive smoothing through frictional wear (Sagy and Brodsky, 2009; Brodsky et al., 2011). Alternatively, large-scale roughening could be the result of fault linkage and the formation of subsidiary faults (Childs et al., 1996; Candela et al., 2009; Candela and Renard, 2012). All of these models have a commonality in that they are characterised by episodic delocalisation and fault zone dilatation followed by failure and frictional wear, which can be preserved in discrete fault rock assemblages. The spatial distribution of fault rock types is important to the present-day hydrologic properties of individual fault zones, which can be calculated in situ, whereas the mechanism of fault slip and the processes of fault growth have important implications for the fluid flow history, and previous transient fluid flow properties, of the fault.

Fault slip is recognised as a trigger for fluid pressure transients (e.g. Wibberley et al., 2008; Faulkner et al., 2010; Bense et al., 2013), which may destabilise the fault and lead to extensive failure (Byerlee, 1993). Equally, a progressive decrease in permeability and fluid pressurisation during creep can promote fault slip. Recent studies by Callahan et al. (2020) and Proctor et al. (2020) highlight how fluid flow can become the dominant driver of fault evolution and stability, as a complication beyond slip zone geometry or rate-and-state friction effects. For example, fluids can exert a direct control on stability by modulating the effective stress field acting on the fault zone, as has been well established elsewhere (e.g. Byerlee, 1990; Sleep and Blanpied, 1992; Ougier-Simonin and Zhu, 2015; Faulkner et al., 2018; Proctor et al., 2020). At the macroscopic scale, faults can trap fluids and maintain near lithostatic internal fluid pressure throughout the entire brittle domain (Byerlee, 1990). In complex fault zones, heterogenous permeability distribution may lead to fluid pressure compartmentalisation within the fault zone (provided the strength of the seal is not exceeded), making them more or less prone to failure (Byerlee, 1993). Localised failure of one compartment may result in propagation of the fluid-pressure transient through neighbouring compartments, causing runaway failure of the fault, as well as allowing intermittent fluid flow through the fault zone in a process known as fault valve behaviour (Sibson, 1990; Byerlee, 1993). On a smaller scale, low-permeability granular rocks such as cataclasites and gouges can experience fluid pressure peaks during shear as they cannot drain fast enough to compensate for

internal porosity destruction during deformation. Here too, a transient fluid pressure increase can lead to dynamic weakening (Ikari et al., 2009; Faulkner et al., 2018).

Alternatively, fluids may contribute to fault strengthening, by catalysing the dissolution-precipitation reactions of fault healing (Gratier, 2011). In natural fault zones, these processes lead to cyclic activity recorded in overprinting generations of fault rocks. The faults commonly have a high inherent structural heterogeneity with anastomosing slip zones enclosing breccia lenses, leading to compartmentalisation (Faulkner et al., 2003; Caine et al., 2010). Fluid pressure transients trigger failure and slip (Sutherland et al., 2012), followed by dilatancy and mineralisation (Caine et al., 2010; Sutherland et al., 2012; Callahan et al., 2020). Restrengthening through cementation may facilitate slip migration into adjacent, relatively weaker structures, but also primes the fault for a next failure (Caine et al., 2010; Gratier, 2011; Sutherland et al., 2012; Callahan et al., 2020).

2.2 Geology and Faulting in the Faroe Islands

The Faroe Islands are an archipelago situated between the Shetland Islands and Iceland, on the European continental shelf of the NE-Atlantic Ocean (Figure 1A). The Faroe Islands are a subaerial remnant of the Paleogene North Atlantic Large Igneous Province, resulting from the initial outburst of the Icelandic Plume before the onset of Atlantic rifting (Ritchie and Hitchen, 1996). The islands are composed mainly of basaltic rocks of the Faroe Islands Basalt Group, which extends for over 200 km to the E and SE of the archipelago (Passey and Bell, 2007; Passey and Jolley, 2008). The Faroe Islands Basalt Group has a maximum stratigraphic thickness of ca. 6.6 km, inferred from the slightly dipping surface exposure and the Lopra-1/1A borehole on Suðuroy (Waagstein et al., 1984; Chalmers and Waagstein, 2006; Passey and Bell, 2007). However, more recent seismic studies point towards a lower maximum thickness of only about 3–4 km under the islands (Ólavsdóttir et al., 2017). The Faroe Islands Basalt Group is subdivided into seven formations that record several periods of volcanic activity with a transition from submarine hyaloclastites to subaerial lavas, interspersed with volcaniclastic deposits recording periods of volcanic quiescence (Passey and Jolley, 2008). A detailed characterisation of the stratigraphy of the Faroe Islands is provided by Passey and Jolley (2008). Initiation of volcanic activity is placed between 60.1 Ma and 55.8 Ma (Hansen et al., 2002; Waagstein et al., 2002; Storey et al., 2007; Passey and Jolley, 2008), with volcanic cessation before 54.5 Ma (measured in correlated units in Greenland and the Faroe-Shetland Basin: Larsen et al., 1999; Hansen et al., 2002; Larsen and Tegner, 2006).

The structural evolution of the Faroe Islands is dominantly influenced by the opening of the NE-Atlantic Ocean. Pre-breakup to post-breakup deformation was characterised previously as a sequence separated into six tectonic stages, recorded by cross-cutting brittle structures on the islands, and which accommodated a progressive vertical axis rotation of the horizontal extension vector (Walker et al., 2011). This stress/strain rotation is interpreted to represent the growth of a continental relay zone between the NE-advancing Reykjanes and SW-advancing Aegir Ridges, with an eventual switch to shortening as a result of abandonment of the Aegir Ridge in favour of the Kolbeinsey Ridge north of Jan Mayen (Gaina et al., 2009; Walker et al., 2011; Gernigon et al., 2012; Ellis and Stoker, 2014; Bubeck et al., 2017). Deformation was accommodated initially by dip-slip faults and conjugate dykes accommodating NE-SW extension (tectonic stages 1–2 respectively), then by conjugate dykes and strike-slip faults accommodating N-S extension (tectonic stages 3–4 respectively), followed by NW-SE extension on strike-oblique slip faults (tectonic stage 5) (Walker et al., 2011). Late-stage overprinting deformation (tectonic stage 6) is also evidenced by the reactivation of tectonic stage 1–5 structures, perhaps as a result of post-breakup passive margin uplift (Walker et al., 2011). Early deformation overlaps with the last stages of basalt emplacement as continental rifting began around 55–53 Ma, and tectonic activity continued at least into the mid Miocene (Roberts and Walker, 2016; Ólavsdóttir et al., 2017).

In many cases, faults and dykes in the Faroe Islands are expressed by deeply incised gullies. Most notably this includes the multiple NW–SE to N–S trending fjords that separate each of the northern islands, which mark the positions of tectonic stage 1–2 faults and dykes (e.g., the Brynhild and Westray fault zones, shown in Figure 1B; Ellis et al., 2009). Tectonic stage 2 faults and dykes also feature prominently in the topography and bathymetry of the Faroe Islands, such as the ESE–WNW striking Skopanafjorður fault (Figure 1B) (Passey, 2009), which separates the northern and southern islands, and an unnamed ENE-WSW structure that caps the northern extremity of the archipelago (Walker et al., 2011). We focus here on three fault zones in the Faroe

Islands (Figure 1B), which are inferred to represent three different displacement scales, from tens-of-metre scale to potentially kilometre-scale displacement.

The inferred smallest displacement fault in the study is located at Í Botni, on the southern island of Suðuroy (Figure 1B). The 30 m displacement at Í Botni can be measured directly from the offset of stratigraphic horizons, and accounts for the plunge of slickenlines on the surfaces of exposed slip zones. Í Botni is a N–S striking fault associated with tectonic stage 1 (Walker et al., 2011), and is hosted in the extensive sheet lobes of the Beinisvørð Formation.

The inferred middle-displacement fault is at Gøtugjógv, Eysturoy (Figure 1B): an ESE–WNW striking sinistral strike-slip fault associated with tectonic stage 4. The Gøtugjógv fault zone forms a prominent lineament that can be traced across the island of Eysturoy, and westwards across the island of Streymoy. The fjord between these two islands marks the position of the Brynhild fault, which is offset across the trace of the Gøtugjógv fault (Figure 1C), from which we estimate a sinistral displacement of up to ca. 500 m. At the position of exposure studied here, the Gøtugjógv fault is hosted in thin compound lavas of the Malinstindur Formation.

The inferred largest fault is an E-W to ESE–WNW striking fault zone at Selatrað, Eysturoy, which is also associated with tectonic stage 4. As with the Gøtugjógv fault, the Selatrað fault is associated with an offset of the bathymetric lineament of the Brynhild fault, between Eysturoy and Streymoy, from which we estimate a sinistral displacement up to ca. 1.5 km. This would make the Selatrað fault one of the largest faults exposed on the islands. At the present level of outcrop, the Selatrað fault is hosted in thin compound lavas of the Malinstindur Formation, and thick simple lavas of the Enni Formation.

Each of the three fault zones exhibits large amounts of smectite and heulandite with minor analcime and chlorite within the fault rock, placing them at a likely depth of around 1–2 km while they were active (Frey et al., 1991; Neuhoff et al., 2000; Jørgensen, 2006). The timing of fault activity for tectonic stage 4 faults (e.g., Selatrað) is constrained by U–Pb dating of calcite cements (Roberts and Walker, 2016), which returned mid Eocene dates (44.8–40.1 Ma). A tentative, and significantly younger, early Miocene (19.4 ± 3.0 Ma) measurement for Gøtugjógv (*see Supplementary data from* Roberts and Walker, 2016) could indicate either long term permeability preservation or hint at long-lived and/or periodic fault activity. Tectonic stage 1 faults (including Í Botni) did not return U–Pb ages, but stratigraphic thickness variations across the fault zones indicate syn-volcanic deformation (Passey and Bell, 2007; Ellis et al., 2009; Walker et al., 2011).

3 Fault Zone Architecture

3.1 Í Botni

The fault zone at Í Botni (IBO, Figure 2) accommodates about 30 m E-down displacement, and is composed of multiple arrays of steep (60–80°) faults distributed over a ca. 50 m thick zone. As highlighted by a red clay marker horizon (blue line in Figure 2C), the majority of the displacement is accommodated across the easternmost fault strand. The steep topography of the outcrop and its proximity to the shoreline renders most of the fault zone inaccessible. Fortunately, the lower few tens of metres of the easternmost fault core have some accessible sections. Here, the fault core is ≤50 cm thick, consisting of grey to light brown, chaotic breccia, gouge, and some cataclasite (fault rock nomenclature from Woodcock and Mort, 2008) bounded by striated and polished black slip surfaces (Figure 2D). These structures are bound by similar but cohesive fine-grained chaotic breccia and cataclasite, which grade to coarser breccias and eventually undeformed host rock to either side.

3.2 Gøtugjógv

The Gøtugjógv fault zone (GOT, Figure 3) is exposed in a 50 m long and up to 10 m high rock face that reveals a section through the 2–3 m thick fault core, from the hanging wall damage zone in the west to the footwall in the east (Figure 3). The exposed damage zone consists of crackle breccia with clasts that gradually coarsen away from the core, and is about 10 m thick in the hanging wall and 3 m thick in the footwall. Veins or cement in the damage zone are rare and limited to thin zeolite veins and calcite or zeolite mineralisation

on slip surfaces. As with the damage zone, the ca. 3 m thick core (comprised of multiple slip zones) has an asymmetric structure in the exposed section. The most prominent slip zone cuts through the fault core in direct contact with the hanging wall damage zone (Figure 3C & Figure 4B), and consists of foliated and unfoliated cataclasites hosting a smooth slip surface, with an average orientation of 194/56° (dip azimuth/dip angle) and slickenlines plunging 104/08° (azimuth/plunge angle) (Figure 4E). This slip surface is corrugated at the metre scale, with corrugations exposed over the 10 m high outcrop. As indicated in Figure 4, the corrugations represent individual lenses of fault rock separated by networks of thin cataclastic shear bands and/or discrete slip surfaces. Lenses contain either breccias or cataclasite, the latter being more prevalent along the prominent slip surface. The transition from breccias and coarse protocataclasites to highly comminuted (ultra-) cataclasites is usually distinct (across a surface) but in places is also gradual. Further away from the slip surface the fault rock lenses increase in size, and potentially cover the entire exposed rock face. Thicknesses of cataclastic shear bands range within the centimetre scale. The core also hosts abundant zeolite and calcite veins, with tabular veins along cataclastic shear bands, either following the contacts or within the bands. Veins are, in places, stacked as 5–10 cm thick composite structures, especially closer to the footwall cut-off (Figure 3D), or as swarms of millimetre-aperture veins. The thick composite veins feature well-developed slickensides between individual veins and on their contacts with the wall rock (Figure 3D). Tabular veins are dominantly parallel, or orthogonal to the main fault orientation.

3.3 Selatrað

The Selatrað fault zone (SEL) is exposed in a <30 m deep and 600 m long gorge separated into two tiers—deeper in the west and shallower in the east—by a waterfall ca. 200 m from the western end. Most of the ca. 7 m thick fault core lies underneath the river carving the gorge. Several anastomosing slip zones enclosing breccia lenses are exposed (Figure 5D). The most prominent slip zone dips northward and can be traced along the southern edge of the gorge (i.e. the footwall) in the upper eastern tier of the gorge, then curves towards the northern edge (i.e. the hanging wall) as the gorge deepens into the lower western tier at the waterfall seen in Figure 5E. This very well-defined smooth surface exhibits centimetre to decimetre wavelength subhorizontal slickenlines along its entire exposure, representing a slip zone that can be traced along much of the gorge. On the upper tier, the slip surface bounds a 5–10 cm thick ultracataclasite. In the lower tier exposures, the slip surface either bounds a similar ultracataclasite layer, or a coarser and less cohesive cataclasite that grades into a chaotic breccia a few centimetres away from the slip surface. An anastomosing network of large secondary faults runs parallel to the slip zone and compartmentalises the fault core into a network of fault-bounded lenses (Figure 5E & F). These lenses are much less altered (e.g., some plagioclase identified in optical microscopy) and fragmented than the bounding cataclastic shear bands. Figure 5F is a map view of one of these lenses, showing internal fragmentation by fractures in Riedel configuration and dominated by R shears (see Figure 6 for illustration of Riedel shears). Similarly, large secondary faults are abundant in the damage zone, and are usually defined by a distinct and continuous corrugated slip surface sandwiched between a centimetre-thick layer of cataclasite to either side. Veins and cements are abundant in the core, but virtually absent from the damage zone. The average main fault orientation measured along the gorge floor is 000/71° with slickenlines plunging 088/08°. However, the slightly less steep topographic orientation of the gorge (ca. 000/60°) may be more indicative of the overall fault zone orientation.

3.4 Fault & Fracture Orientation

Different measuring techniques were required to extract fault orientation data at different scales, including: in the field, virtual outcrop models, and orthophotos. This approach could introduce scale- and method-dependent biases, hence we only compare the three fault zones qualitatively. In Gøtugjógv and Selatrað fault orientation has been measured in the field and reconstructed from the UAV-derived 3D virtual outcrop models (Figure 7). The orientation of an assumed uniform fault plane can be estimated from its intersection with the topography of the 3D outcrop surface. For this, fault traces were picked in 3D photogrammetry models of the fault zones, and a plane was fitted to these traces so that it would contain a maximum of vertices from the picked fault trace line. This method incurs uncertainty because: (1) the intersected rock faces generally have little relief, and fitting planes to fault traces is therefore dependent on the accuracy of the modelled surface and the position of the picked lineament; and (2) minor-displacement (millimetre–centimetre scale) fault surfaces may be composite structures that are below the resolution of the models. For instance, Walker et al. (2012) showed that surfaces of millimetre–centimetre scale displacement faults associated with tectonic stage 4 comprised linked faults and fractures that ranged in strike from ca.

060°–115° on a fault with an overall strike of ca. 060° (e.g., their figure 4). We also report a lineament analysis on orthophotos of a close-up of the Selatrað gully floor (Figure 5F-G), which is almost flat, hence we are confident that fault traces are representative of fault strike, accurate to within ca. 5°.

The large-scale structure of the fault core and damage zone are strongly dominated by faults in Y to R orientation (see Figure 6 for an illustration of Riedel shears), as well as subordinate P faults (Figure 7). High angle shears (R' and X) are much less common and, in the case of the Selatrað fault core (Figure 5F), occur mostly as relatively late-stage structures that either fragment large clasts bounded by low-angle faults, or transect all other structures. We see similar high angle shears that transect the Gøtugjógv slip zone. This pattern is repeated on a smaller scale in centimetre- to decimetre-sized hand specimens, especially in foliated cataclasite (Figure 8B). Here R and P shears define a well-developed foliation bounded by fault-parallel Y shears separating different types of fault rock (e.g., ultracataclasite from cataclasite). Late-stage high-angle R'- and X-parallel shears cut through these boundaries as well as the foliation. Notably, the sense of slip along some of these high-angle shears is opposite to the sense of slip that would be expected for R' and X shears developed in simple shear (Figure 6), possibly indicating a pure shear (i.e., flattening) component to deformation.

4 Fault Rock Characterisation

4.1 Í Botni

Damage concentration changes drastically over a very narrow zone in the ca. 30 m displacement fault zone of Í Botni. The slip zone consists of a centimetre-wide swarm of anastomosing sub-millimetre thick, black, polished slip surfaces with clayey cataclasite in between (Figure 2D). The slip zone is directly adjacent to crackle and chaotic breccias, that comprise largely unaltered basalt clasts in an authigenic cataclastic matrix (Figure 8A, Figure 9 IBO-i & ii, Figure 10A) on one side, and cataclasite or gouge with few relict clasts on the other side (Figure 9 IBO-iv). Initial XRD analyses (in digital supplement) show plagioclase and pyroxene to be preserved throughout most of the fault zone.

4.2 Gøtugjógv

4.2.1 Breccias & Veins

Breccia veins in the Gøtugjógv fault core are mostly composed of angular and poorly sorted clasts suspended in a mineral cement of either calcite or, more commonly, zeolite (Figure 8E-G, Figure 9 GOT-iv - x). Clast concentration in these breccia veins varies considerably, from domains that are potentially clast-supported to domains that are pure mineral vein (i.e., without clasts, Figure 11). Angular clasts ranging from sub-millimetre to centimetre scale are hosted in a cement of <50 μm long acicular to bladed zeolite, or equant calcite measuring a few millimetres across. The zeolite cement has a weak, apparent shape-preferred orientation (SPO) forming a cross-shaped texture with axes at a 45° angle with the vein boundaries (Figure 10E). A similar apparent SPO can be seen in the matrix of some cataclasites (Figure 10F and paragraph below). The veins also contain numerous millimetre-sized pockets of irregular shape, with idiomorphic zeolite crystals protruding from the cement and commonly filled with a single crystal of calcite (Figure 9 GOT-viii & x, Figure 10E). Similarly, clasts of wall rock in calcite-cemented breccias are commonly lined with syntaxial idiomorphic zeolite, and the cement contains millimetre-sized pockets of zeolite. The clast population includes altered host rock (Figure 9 GOT-iv & v), reworked fault rock (Figure 9 GOT-ix & x), and in some cases larger fragments of older veins or cement (Figure 9 GOT-vii).

Similarly, small non-tabular veins can be observed in the domains further away from the most prominent slip zone and especially in thicker cataclasite bodies. These zones are predominantly cemented by syntaxial bladed or blocky zeolite with a wide range of crystal sizes, and equant calcite mineralisation is also common. Their shape and orientation is irregular, frequently splaying, merging, and diverging, with variable aperture and orientation, with the wider segments hosting small fragments of wall rock (Figure 8G, Figure 9 GOT-xi). We interpret the clast angularity paired with the dominance of mineral cement over matrix as strong evidence for breccia veins originating from hydrofracture and implosion (see Jébrak, 1997).

Some outcrop-scale breccia pods are characterised by a more chaotic texture than the previously described breccia veins: Their clasts are sub-angular to rounded with less distinct edges. Clast concentration varies greatly, and they are hosted in a mixture of zeolite and clays. Clay matrix concentration in the cement is high, but varies across centimetre-scale patches (Figure 8D, Figure 9 GOT-vi).

Many areas, especially along the contacts of different fault rock units, host centimetre-wide multiphase swarms of thin zeolite and calcite veins. Veins appear to exploit the vein walls or wall rock directly adjacent to previous veins, rather than forming within each other, though examples of cross-cutting veins are observed. Veins and breccia cements record either extensive or no internal strain from reshearing of the fault, as evidenced by twinning, inter- and intracrystalline cracking, and grain size reduction. Where interfaces host slickensides, the outer few millimetres of cement are comminuted and separated from the unstrained inner layer by Y shears, as seen in Figure 9 GOT-viii.

4.2.2 Cataclasites

The textural transition from breccia to cataclasite and ultracataclasite is gradual (Figure 11). On the coarse end of the scale, cataclasites resemble the unorganised breccias described above. They have sub-angular to rounded clasts of fault rock and altered host rock hosted in a comminuted and slightly altered, authigenic matrix with sparse, unconnected and irregularly shaped patches of cement (Figure 8B, Figure 9 GOT-ii). Finer cataclasites host fewer clasts, and the composition of those clasts is dominated by polycrystalline zeolite aggregates without clay, in a matrix of homogeneous zeolite, pyroxene, and clay (Figure 8C & G, Figure 9 GOT-iii & GOT-xi, Figure 10D, G & H). In some cases, the zeolites have an acicular habit defining a lattice-shaped apparent SPO inclined to the slip plane, similar to zeolite cement in veins (Figure 10F). In the hanging wall slip zone, the clay minerals show a distinct foliation. Mesoscopic foliation is defined by millimetre thick clay bands parallel to the R, P, and Y orientation (Figure 8B, Figure 9 GOT-ii) and only developed in the coarser cataclasite further from the slip surface. Microscopic foliation is defined by very thin and continuous clay bands at a higher angle to the slip surface (40–55°), with the foliation only developed in the ultracataclasite (Figure 10G & H). Late-stage high-angle fractures (red in Figure 8B) commonly transect and offset all other structures, layer boundaries (i.e., ultracataclasite to cataclasite), foliation, and other shear bands/fractures. They are parallel to the R' orientation but their sense of shear can be both synthetic and antithetic, which we interpret as a combination of potential compactional/pure shear (synthetic) and rotational/simple shear (antithetic) components of deformation (Figure 6). Further, SEM-BSE imaging shows that the cataclasites maintain a significant porosity even where highly strained (Figure 10I).

4.3 Selatrað

The sampled ultracataclasite which constitutes the slip surface (Figure 9 SEL-iii) is texturally very similar to the abandoned red clay ultracataclasite from the Gøtugjógv fault core (Figure 9 GOT-xi). It has not been brecciated, nor cut by zeolite veins, but the texture is nearly identical, showing a red clay-dominated matrix with very fine-grained pyroxene fragments and larger polymineralic clasts. Many of these clasts contain calcite, and calcite vein fragments can be identified indicating prior stages of veining within the fault. The weakly consolidated cataclasite that can be found along parts of the well exposed slip surface in the lower tier, is dominated by a red clay matrix and contains polymineralic clasts that can be up to 5 cm across, but are more commonly sized at the millimetre scale. Clast concentration gradually increases away from the slip surface and the rock can be classified as mosaic breccia ca. 30 cm from the slip surface. Consequently, the internal structure of fault rock lenses is dominated by mosaic and crackle breccias with a systematic fragmentation along R to R'.

As mentioned above, secondary faults in the damage zone are separated by cataclasite layers to either side. The cataclasites are usually only a few centimetres wide, even for extensive and polished slip surfaces. Boundaries to the undeformed wall rock can be sharp or gradual. The cataclasite layer is strongly altered. In the case of the fault zone-oblique narrow cataclastic band in Figure 9 (SEL-i), the assemblage has completely changed to zeolite and remnant pyroxene, with an undulating boundary back to unaltered wall rock expressed by linkage of R and Y shear planes. The fault zone-parallel and slightly wider slip zone in Figure 9 (SEL-ii) grades from a zeolite- and clay-dominated cataclasite on the left through a brecciated zone with angular and weakly altered wall rock clasts in a zeolite cement. Throughout the damage zone, basalt wall rocks show only minor, or no alteration.

5 Discussion

5.1 Fluid Flow & Chemical Alteration

Pervasive alteration in the fault zone is limited to fractured rocks (Figure 9 IBO-i - ii, SEL-i, GOT-i & Figure 10A), which we infer is the result of damage-enhanced fluid flow. The fault rocks from the low displacement fault in Í Botni preserve an original plagioclase-pyroxene assemblage in most samples, with the only exception being the heavily altered and reworked footwall breccia (Figure 9 IBO-iii). Hanging wall breccias in direct contact with the slip surface show alteration penetrating no more than 0.1–0.5 mm into clasts (Figure 9 IBO-i - ii). Likewise, in the Gøtugjógv and Selatrað damage zones, alteration is limited to fracture and vein walls (Figure 9 GOT-i, GOT-xii, SEL-i & Figure 10B), which may reflect the very low permeability ($<10^{-20}$ m^2) of intact Faroe Islands basalts (Walker et al., 2013a; 2013b). This is contrasted by the complete textural and mineralogical breakdown observed in the Gøtugjógv and Selatrað fault cores, which are composed of a clay-zeolite assemblage with remnant pyroxene (e.g., Figure 9 GOT-ii, GOT-vi, GOT-xi, SEL-iii). Wall rock clasts entrained in the core consistently show strong alteration, even though primary texture may be preserved (Figure 9 GOT-iv & Figure 10C). The inferred alteration sequence is in line with permeability variation measured along basaltic faults in the Faroe Islands. Walker et al. (2013a; 2013b) recorded elevated permeability in the fault cores, which are enclosed laterally by low-permeability damage zones; this configuration promotes fault-parallel fluid channelling.

Fault core permeability has been shown to be strongly linked to the interplay between comminution and clay generation (permeability reduction), and the establishment of interconnected and porous (zeolite) vein networks and microdamage (permeability increase) (Sutherland et al., 2012; Walker et al., 2013a), but also to local strain concentration and petrographic heterogeneity along the fault (Caine et al., 2010; Sutherland et al., 2012). For example, low-porosity clay-dominated cataclasite or gouge is probably more readily sealed than zeolite-dominated chaotic breccia (Walker et al., 2013a). The integrity, continuity, and abundance of veins, mineralised breccias, and clay-dominated shear bands varies strongly throughout the mature fault zones in Gøtugjógv and Selatrað, which should lead to significant permeability variations within the fault zones. Fault rock assemblages in the larger displacement faults are lens-shaped, hence have the potential to be fully enclosed by low permeability clay-dominated slip systems. This geometry of heterogeneous fault rock could therefore promote compartmentalisation and fluid pressure variations along the fault zones, depending on the volume of entrapped fluid and the degree of local compaction (Byerlee, 1993; Caine et al., 2010; Sutherland et al., 2012). Such a configuration should lead to local overpressurisation and hydrofracture, and could explain the mutual overprinting of structures recording cataclasis and hydrofracture in Gøtugjógv. Hydrofracture is unlikely to happen simultaneously along the entire fault, and therefore could cause fluid pumping and considerable transient effective stress variations, potentially triggering failure, as noted elsewhere (Byerlee, 1993; Eichhubl and Boles, 2000; Caine et al., 2010; Warren-Smith et al., 2019; Callahan et al., 2020). As with compartmentalisation leading to fluid pressurisation on a large scale, low permeability fault rocks can be susceptible to dynamic internal pressurisation on a much smaller scale. Their low permeability can prevent fluids from draining from the rocks to equilibrate pressure increases related to porosity destruction during shear-compaction (Sleep and Blanpied, 1992; Ikari et al., 2009; Faulkner et al., 2018). Combined, fluid trapping and pressurisation may provide a mechanism for fluid pressure cycling and repeated mineralisation events in the fault zones, without the need for a maintained external fluid supply for pressure transients. In this scenario, mineral alteration and replacement would be largely driven by fault-internal redistribution, without considerable net loss or gain of chemical species.

Most of the cataclasites studied have a very high zeolite concentration in their matrix as well as abundant zeolite and calcite vein fragments. It might be difficult to account for such high zeolite concentrations from a mass balance perspective without the influx of external fluids. A significant portion of matrix zeolite could derive from secondary mineralisation and not just from reworking of zeolitised host rock. In that case, zeolite would be progressively added to the fault zone, either through precipitation in veins and breccias over several mineralisation cycles, or by continuous precipitation into microporosity opened during dilatant cataclastic flow (Stel, 1981; Hadizadeh and Foit, 2000). Both processes for secondary mineralisation could contribute to the high zeolite concentration and would necessitate an active fluid circulation.

5.2 Fault Core Widening

Fault core thickness of the three faults studied here increases from about 0.5–1.0 m in Í Botni (30 m displacement), to 2–3 m in Gøtugjógv (up to ca. 500 m displacement), and 7 m in Selatrað (up to ca. 1.5 km displacement). These values consistently range on the higher end of fault core thickness relative to displacement compared to scaling relationships for other faults (Shipton et al., 2006; McKay et al., 2021). The displacement-thickness ratios (D/T) for faults in this study follow $T = 0.1D^{0.56}$ compared to $T = 0.025D^{0.65}$ calculated by McKay et al. (2021). However, it should be noted that (1) our dataset is based on only three faults, (2) thicknesses from our study may not represent the maximum thickness, and (3) there is significant scatter in D/T plots based on large datasets. Hence, we do not seek to quantitatively explore this relationship further, here. Observations from the three faults in the Faroe Islands do, however, suggest that once fault zones in basalts have accommodated displacements at the tens-of-metre scale (e.g., Í Botni), further displacement may be accommodated by fault core thickening, or by reworking of existing fault rock, potentially involving no thickness change, or even a reduction in thickness. Individual slip zones are a relatively consistent thickness (5–10 cm). In contrast, the preserved fault core thickness at a given locality is expected to be highly variable, dependent on several factors including (but not limited to): (1) the number of slip events recorded; (2) the position of those events, relative to previous events; (3) the nature of those slip events (shear zone thickening or thinning); and (4) fluid-mediated dilatation, alteration, and mineralisation. The three faults studied here, show a complex evolution for individual faults, but are controlled by common processes, which apparently become dominant beyond tens-of-metre scale displacements.

The complex internal geometry, with strong strain partitioning between brecciated lenses and cataclastic shear bands suggests repeated assimilation of less deformed wall rock into the fault core. Callahan et al. (2020) recently proposed combined fluid-driven cyclic dilatation and mineralisation, alternating with embrittlement and shear deformation, as well as damage zone assimilation during fault core stepping, as widening processes for the Dixie Comstock fault. This process has also been inferred for the Stillwater fault, which is part of the same system (Caine et al., 2010). We see evidence of both processes in the Faroe Islands fault zones. For instance, a mineralisation-deformation cycle is supported by thick veins and widespread mineralisation in the Gøtugjógv core and abundant fragments of reworked older veins in fault rocks. Wall rock ablation may be recorded by relatively unaltered wall rock fragments with preserved textures found in low strain lenses. Following integration into the fault core, these lenses were probably fragmented and assimilated through frictional wear processes (as described in Sagy et al., 2007; Childs et al., 2009; Brodsky et al., 2011). The widespread occurrence of heavily altered fault rock fragments derived from frictional shear within mineralised portions of the Gøtugjógv fault most likely indicates that alteration weakening did not promote the development of a stable permanent slip zone, in contrast to the inferred development of the Dixie Comstock fault (Callahan et al., 2020). There are several potential mechanisms for internally driven fault core migration, which we will discuss in more detail below. However, wall rock ablation can also be driven externally through linkage of fault segments and secondary faults, cutting off large lenses of damage zone rock as well as introducing slip surface corrugation of the same geometric scale as the wall rock lenses (Childs et al., 2009; Candela and Renard, 2012). This process appears to be dominant at earlier stages of fault zone evolution, as seen in the wide and low displacement fault zone at Í Botni.

5.3 Slip Zone Locking & Migration

Reworked clasts of cataclasites within the fault cores and the multitude of distinct, variably reworked slip zones require episodic principal slip zone (PSZ) migration. This implies that previously active slip zones became unfavourable for continued slip, despite the development of relatively weak clay assemblages: i.e., they became locked. The fault rock (micro-) structure provides evidence for several processes that might have contributed to slip zone hardening and locking, which are outlined below:

(1) Principal slip zone & slip surface dissection: High-angle shears dissecting strain-concentrating structures, juxtaposing low-strength and high-strength structures, e.g. clay foliation and zeolite matrix or gouge and cataclasite (Figure 8B), could increase the bulk strength of the slip zone and result in PSZ locking. Should these high-angle shears form during slip, they would have to accumulate their small displacements at a faster rate than the slip rate accommodated across the slip zone to prevent bypassing or progressive removal and incorporation of any emerging asperities into the adjacent gouge/cataclasite layer. More likely, we infer the observed high-angle shears developed in one of two scenarios: (1) during post-slip creep, forcing

subsequent slip to relocate into another structure, or (2) during fragmentation of an embrittled and abandoned slip zone in the vicinity of a new PSZ. Sagy and Brodsky (2009) identified similar layer transecting structures as an important process for re-roughening in mature slip zones and proposed that they are a type of boudinage structure emerging from the rheological contrast developed as a consequence of strain-hardening in the cataclasite/gouge layer. Applied to the structures observed in the Faroe Islands, the Riedel shears would record segmentation into shearband boudins by simple shear, while the opposite-sense shears would record compaction of boudins in pure shear.

(2) Zeolite recrystallisation: The zeolite apparent SPO recorded in some cataclasite, resembling the apparent SPO observed in veins (Figure 9E & F), could imply a similar process of formation. It is unlikely that zeolites in the cataclasites could maintain an elongated habit during cataclasis, as their shape would be expected to inhibit grain rotation necessary for granular flow in cataclasite and gouge. The apparent SPO is more likely a result of dynamic or static recrystallisation, which could also have affected zeolite veins. Material science studies have shown that many natural and synthetic zeolites readily dissolve and reprecipitate in alkaline conditions under atmospheric pressure and temperatures below ca. 110°C (e.g. Ivanova and Knyazeva, 2013). This is similar to the conditions thought necessary to favour zeolite over calcite precipitation in Icelandic basalts (Neuhoff et al., 2000). If reactivity in the PSZ is high enough for recrystallisation to outpace comminution, it is also likely to allow for healing of the slip surface during aseismic creep (Renard et al., 2012), leading to overall strengthening of the slip system. However, the observed apparent SPO could also be a result of post-shear static recrystallisation, in which case it would only contribute to strength recovery after a slip event.

(3) Cementation: The prevalence of fresh and reworked veins, hydraulic breccias, and the almost bimodal strain distribution in cements—either intact or highly strained—evidence periodic fluid overpressure and mineralisation in the fault core. Cyclic fluid pressurisation and hydrofracture is commonly observed in both seismogenic (e.g. Byerlee, 1993; Eichhubl and Boles, 2000; Caine et al., 2010; Callahan et al., 2020) as well as slow slip faults (Warren-Smith et al., 2019). As noted above, permeability can drop significantly within high strain gouge and cataclasite, especially in clay-rich assemblages, through porosity compaction. To allow for repeated pressurisation, porosity could be reset by fluidisation during high-velocity slip events (Sleep and Blanpied, 1992; Ikari et al., 2009; Faulkner et al., 2018). While we observed no strong evidence for gouge fluidisation (Monzawa and Otsuki, 2003; Otsuki et al., 2003), the reworking of fault rocks by granular flow after PSZ migration may offer a viable alternative process to reintroduce porosity. In any case, cataclasites clearly show open pore space in SEM-BSE images (Figure 10I) as well as fabric elements most likely recording compaction (e.g. Figure 8B). It is evident that fluids in the PSZ were overpressured and led to extensive hydrofracture. This might have caused a transient decrease of frictional strength, triggering rapid, potentially even seismogenic slip (Byerlee, 1993; Faulkner et al., 2018). Ensuing precipitation of zeolites and calcite could restrengthen the slip zone and potentially shut it down (Caine et al., 2010; Wästeby et al., 2014; Callahan et al., 2020). Even though recent thermodynamic calculations (Williams, 2019) show that pressure-boiling induced by dilation is an unviable process for rapid mineral precipitation, post-earthquake hydrochemical recovery times of 8–10 years measured in Iceland (Wästeby et al., 2014) indicate that rapid precipitation-sealing must be accommodated by other, unknown processes. This is in line with our observation of highly angular clasts in the breccia veins, which could only be preserved if transport related wear were minimal.

(4) Strain-hardening: Smectite-rich gouges have been shown to be dominantly strain-hardening (Saffer and Marone, 2003; Tembe et al., 2010; Boulton et al., 2014; Morrow et al., 2017), which could also significantly contribute to the cyclicity of fault rock production and PSZ migration. Shutdown and migration of cataclastic slip zones as a result of strain-hardening has been proposed for example in the Carboneras fault zone in Spain (Faulkner et al., 2003) as well as the Flowers Pit fault zone in the USA (Sagy and Brodsky, 2009; Brodsky et al., 2011). In this scenario, progressive strain wears down asperities, producing fine-grained material and thickening the cataclastic layer. Smoothing of the slip surface, lubrication by gouge, and strain-hardening in the cataclastic layer lead to slip localisation onto a principal slip surface. Localisation is counteracted by removal of asperities and boudinage-like transection of the embrittled cataclasite layer, deforming and re-roughening the adjacent slip surface, thus allowing continuous reworking and generation of gouge/cataclasite (Candela et al., 2009; Sagy and Brodsky, 2009; Brodsky et al., 2011). Such a process could explain gouge/cataclasite production in fault sections without extensive mineralisation such as those exposed in Selatrað.

5.4 Fault Strength

Fault strength is governed by the interplay between fault structure and rock mechanics, chemical influences, and episodic effective stress variations (Faulkner et al., 2010). Local structure is a first order control as the distribution and geometry of slip surfaces and fault rocks influence strain partitioning within the fault zone (e.g. Moore and Byerlee, 1992; Faulkner et al., 2003; Caine et al., 2010; Gratier, 2011; Renard and Candela, 2017). The generation of thick layers of cataclasite around a relatively smooth principal slip surface provides evidence for shear localisation within the PSZ. Strain is most likely transferred gradually from distributed granular flow within the cataclasite (or even breccias) in a newly established slip zone, onto a localised smooth slip surface later in the cycle. This would imply a general strain-hardening behaviour of the cataclasites (Sagy and Brodsky, 2009), probably as an effect of progressively reduced grain size (Eberhardt et al., 1999), and increasing clay concentration (Tembe et al., 2010; Haines et al., 2013).

The chemical control on fault rock strength is defined by the opposing influences of alteration-weakening and cementation-strengthening (Caine et al., 2010; Callahan et al., 2020). The introduction of fluids into the fault zone most likely leads to the observed chemical breakdown of strong plagioclase into clays and zeolite, characterised by a significantly reduced mechanical strength (e.g. Saffer and Marone, 2003; Tembe et al., 2010; Yukselen-Aksoy, 2010; Frolova et al., 2014; Morrow et al., 2017), thus permanently weakening the rock. In the evolved fault rocks described above, the chemical influence on strength is probably linked mainly to episodic mineralisation with zeolite and calcite, both in (breccia) veins and disseminated throughout the fault rock. This most likely results in a transient strengthening through the direct effect of cementation (e.g. Caine et al., 2010; Callahan et al., 2020), but could also cause a long-term increase in strength if the overall composition progressively shifts towards more zeolite and calcite, relative to clay minerals. Zeolite and calcite veins in the studied faults preferentially exploited pre-existing vein walls or the wall rock directly adjacent to veins. This indicates that cements are stronger than the clay-dominated wall rock or the vein-wall rock interface (Virgo et al., 2013). This is also supported by the presence of well-developed slickensides on the vein interfaces (Figure 3D) showing that shear preferentially localises here before disrupting the veins. It has been shown that the overall efficiency of healing processes active on slip surfaces is promoted by the highly reactive minerals on these surfaces, such as zeolites and calcite in our case, and the catalysing effect of fluids, but is impeded by the less reactive clay minerals (Gratier, 2011; Renard et al., 2012). Analysis of post-seismic fluid chemistry on the analogous Húsavík-Flatey Fault in Iceland shows full hydrochemical recovery, assumed to mirror fracture healing by mineral precipitation, after about 8–10 years even though it is delayed by minor refracturing events (Wästeby et al., 2014). It should be noted though, that mechanical recovery by mineralisation does not necessarily imply full sealing of fluid pathways (Aben et al., 2017).

Immediately before and during slip, the effect of fluid pressure changes imposed by compaction and dilation can exceed the intrinsic frictional characteristics of the fault rock to become the dominant control on fault stability (Proctor et al., 2020). As described previously, compartmentalisation could result in considerable local fluid pressure variation in fault zones. If one such compartment fails, rapid fluid flow may create a fluid pressure transient that would migrate through the fault zone (Byerlee, 1993; Hill et al., 1993; Caine et al., 2010). The associated effective stress drop is recorded by numerous implosion breccias throughout Gøtugjógv, and centimetre-scale calcite crystals in veins, requiring fractures to be maintained open over a substantial period of time, potentially hundreds to thousands of years (Lee and Morse, 1999; Frery et al., 2015). Even in the absence of an external fluid pressure transient, creep of saturated granular fault rock (i.e. gouge or cataclasite) can result in internal overpressure through shear compaction and ineffective fluid drainage from the low permeability rocks (Sleep and Blanpied, 1992; Ikari et al., 2009; Faulkner et al., 2018). In both scenarios the effective pressure reduction entails mechanical weakening (Ikari et al., 2009; Morrow et al., 2017; Faulkner et al., 2018), that might eventually lead to fluid overpressure and hydrofracture. Besides the direct effects on fault shear strength by effective pressure reduction, episodic fluid flow can mediate many of the permanent and transient chemical processes previously described, such as alteration-weakening, mineralisation-strengthening, and healing.

5.5 Fault Zone Evolution

The three fault zones analysed share features of fault damage growth and evolution in basaltic rocks, captured at three different displacement scales. We infer that the main features of these faults can be treated conceptually as progressive stages in the evolution of individual faults in the Faroe Islands basalts in a space-

for-time substitution, and displacement ranges from tens-of-metres scale to potentially hundreds-of-metres- or kilometres-scale.

Based on our observations, we propose a model for cyclic fault evolution, where localised cataclastic flow, probably during subseismic slip or creep, alternates with episodic core embrittlement and extensive hydrofracture and cementation. Our model may be subdivided into seven stages (Figure 12), which are described below. The combined effects of transient changes to permeability and fault strength are illustrated in Figure 13.

Stage 1: Fault zones initiate in arrays of small faults in Riedel configuration—as exemplified in the damage zone of Selatrað (Figure 3 & Figure 7)—which link to create a network of continuous, large faults localising strain (Peacock, 1991; Peacock and Sanderson, 1995; Walsh et al., 2003; Childs et al., 2009; Candela and Renard, 2012; Crider, 2015; Rotevatn et al., 2019).

Stage 2: Continued localisation results in the formation of a cataclastic PSZ that accommodates the majority of displacement across the fault. Damage concentration around the PSZ leads to the progressive widening of the fault core (as seen in Í Botni, Figure 2).

Stage 3: Formation of fine-grained fault rocks in the PSZ and pervasively fractured lenses of damage zone rocks, which comprise a host rock mineralogy dominated by plagioclase and pyroxene, are almost completely replaced by a clay and zeolite assemblage. The timing of fluid-mediated alteration is constrained by the weakly altered Í Botni fault core and local alteration around damage zone fractures in Gøtugjógv and Selatrað (Figure 9 & Figure 10). All three faults should show extensively altered damage zones if alteration had preceded damage concentration.

Stage 4: The reduction in grain size and increase in clay content within the fault core reduces permeability and fluid flow within the fault. Compaction-related increases in fluid pressure cannot be drained from the fault core, which leads to hydrofracture, both as discrete veins and pervasive brecciation, followed by rapid mineralisation (keeping clasts in suspension, Jébrak, 1997) by zeolite and calcite (e.g., Gøtugjógv, Figure 9 GOT-iv - xi), potentially leading to permanent fault core thickening.

Stage 5: Following extensive mineralisation and cementation, renewed slip may relocate into a less cemented domain to form a new PSZ. Refracturing of abandoned older slip zones and subsequent entrainment into the newly forming PSZ results in reworking of previous generations of fault rock, and the formation of clast-within-clast textures (e.g., Figure 8G and Figure 9 GOT-xi).

Stage 6: Fragmentation in the abandoned core follows Riedel orientations, as can be seen in Figure 8B, transecting and offsetting older shear planes. These newly brecciated fault rocks are progressively comminuted and homogenised as they are incorporated into the creeping slip zone.

Stage 7: The slip zone may lock due to a combination of the four processes discussed above: slip zone transection, zeolite recrystallisation, cementation, and strain-hardening. In the fine-grained and homogeneous slip zone, the rock texture resembles that from stage 3 again. Fluid pressure rises, resetting the cycle (stages 3–7).

5.6 Implications for Basalt-Hosted Fault Zones

The processes we infer to play a significant role during fault evolution in the Faroe Islands have all been shown to occur commonly in the shallow crust. Basalts typically break down into zeolites and smectites under hydrous conditions (Seyfried and Bischoff, 1979; Utada, 2001; Gysi and Stefánsson, 2012; Frolova et al., 2014). Cataclastic slip zones commonly develop in crystalline rocks of all kinds (Sagy and Brodsky, 2009; Caine et al., 2010), and are prone to episodic locking and reworking (Faulkner et al., 2003; Sagy et al., 2007; Caine et al., 2010; Callahan et al., 2020) as well as strain-hardening if they contain smectites (Saffer and Marone, 2003; Tembe et al., 2010; Morrow et al., 2017). Similarly, hydrofracture as a consequence of permeability reduction and fluid trapping has been proposed in several fault zones and settings (Byerlee, 1993; Caine et al., 2010) and can develop intrinsically in fault zones without an external fluid pressure source (Byerlee, 1993; Faulkner et al., 2018; Proctor et al., 2020). Furthermore, the simple geological history of the Faroe Islands precludes any strong influence from structural inheritance, or late overprinting of the fault zones (Neuhoff et al., 2000; Walker et al., 2011; Ólavsdóttir et al., 2017). Hence, we propose that our model for fault evolution in the Faroe

Islands could apply more widely to shallow basalt-hosted fault zones in general. Our model expands the displacement scaling for faults in basaltic rocks described in Walker et al. (2012; 2013b) by up to two orders of magnitude, and provides new insights into the evolution stages and processes that might occur within mature basalt-hosted fault zones.

6 Conclusion

Fault zones in the Faroe Islands are interpreted to display repeated principal slip zone migration and fault rock reworking. After an initial phase of permanent chemical weakening promotes strain localisation into a principal slip zone, phases of stable cataclastic shear alternate with hydrofracture followed by pervasive cementation of the principal slip zone. The mechanical properties are governed by an interplay between coeval and successive weakening and strengthening processes: Comminution and increasing clay content in the principal slip zone lead to mechanical weakening through fluid pressure increases, while strengthening processes are either mechanical (in the form of strain-hardening of the granular fault rocks) or chemical (in the case of fluid-mediated cementation and healing). Mechanical and chemical strengthening culminate in locking of the slip zone and force the fault to reorganise around a weaker structure, restarting a new cycle of cataclastic shear. Fluids play a critical role in the structural and mechanical evolution of these faults, through their catalysing effects for chemical alteration of the fault rocks, as a transport medium in dissolution-precipitation processes cementing the fault zone, and in modulating effective stress within the fault zone. We propose that similar processes could govern the evolution of shallow-level, basalt-hosted fault zones in general.

7 Acknowledgments

This work was funded by the College of Science and Engineering of the University of Leicester. We thank the editors, David Fastovsky and Mike Williams, as well as two anonymous reviewers for their suggestions which greatly improved this manuscript.

Uninterpreted versions of figures are available in the digital supplement.

8 References

Aben, F., Doan, M. L., Gratier, J. P., and Renard, F., 2017, Experimental postseismic recovery of fractured rocks assisted by calcite sealing: Geophysical Research Letters, v. 44, no. 14, p. 7228-7238.

Bense, V. F., Gleeson, T., Loveless, S. E., Bour, O., and Scibek, J., 2013, Fault zone hydrogeology: Earth-Science Reviews, v. 127, p. 171-192, https://doi.org/10.1016/j.earscirev.2013.09.008.

Boulton, C., Moore, D. E., Lockner, D. A., Toy, V. G., Townend, J., and Sutherland, R., 2014, Frictional properties of exhumed fault gouges in DFDP-1 cores, Alpine Fault, New Zealand, v. 41, no. 2, p. 356-362, doi:10.1002/2013GL058236.

Brodsky, E. E., Gilchrist, J. J., Sagy, A., and Collettini, C., 2011, Faults smooth gradually as a function of slip: Earth and Planetary Science Letters, v. 302, no. 1, p. 185-193, https://doi.org/10.1016/j.epsl.2010.12.010.

Bubeck, A., Walker, R. J., Imber, J., Holdsworth, R. E., MacLeod, C. J., and Holwell, D. A., 2017, Extension parallel to the rift zone during segmented fault growth: application to the evolution of the NE Atlantic.

Bubeck, A., Walker, R. J., Imber, J., and MacLeod, C. J., 2018, Normal fault growth in layered basaltic rocks: the role of strain rate in fault evolution: Journal of Structural Geology, v. 115, p. 103-120.

Byerlee, J., 1990, Friction, overpressure and fault normal compression: Geophysical Research Letters, v. 17, no. 12, p. 2109-2112.

Byerlee, J. D., 1993, Model for episodic flow of high-pressure water in fault zones before earthquakes: Geology, v. 21, no. 4, p. 303-306.

Caine, J. S., Bruhn, R. L., and Forster, C. B., 2010, Internal structure, fault rocks, and inferences regarding deformation, fluid flow, and mineralization in the seismogenic Stillwater normal fault, Dixie Valley, Nevada: Journal of Structural Geology, v. 32, no. 11, p. 1576-1589, https://doi.org/10.1016/j.jsg.2010.03.004.

Callahan, O. A., Eichhubl, P., and Davatzes, N. C., 2020, Mineral precipitation as a mechanism of fault core growth: Journal of Structural Geology, v. 140, p. 104156, https://doi.org/10.1016/j.jsg.2020.104156.

Candela, T., and Renard, F., 2012, Segment linkage process at the origin of slip surface roughness: Evidence from the Dixie Valley fault: Journal of Structural Geology, v. 45, p. 87-100.

Candela, T., Renard, F., Bouchon, M., Brouste, A., Marsan, D., Schmittbuhl, J., and Voisin, C., 2009, Characterization of fault roughness at various scales: Implications of three-dimensional high resolution topography measurements, Mechanics, structure and evolution of fault zones, Springer, p. 1817-1851.

Carpenter, B. M., Ikari, M. J., and Marone, C., 2016, Laboratory observations of time-dependent frictional strengthening and stress relaxation in natural and synthetic fault gouges: Journal of Geophysical Research: Solid Earth, v. 121, no. 2, p. 1183-1201.

Chalmers, J. A., and Waagstein, R., 2006, Scientific results from the deepened Lopra-1 borehole, Faroe Islands, Geological Survey of Denmark and Greenland, Danish Ministry of the Environment.

Childs, C., Manzocchi, T., Walsh, J. J., Bonson, C. G., Nicol, A., and Schöpfer, M. P. J., 2009, A geometric model of fault zone and fault rock thickness variations: Journal of Structural Geology, v. 31, no. 2, p. 117-127, https://doi.org/10.1016/j.jsg.2008.08.009.

Childs, C., Nicol, A., Walsh, J. J., and Watterson, J., 1996, Growth of vertically segmented normal faults: Journal of Structural Geology, v. 18, no. 12, p. 1389-1397.

Crider, J. G., 2015, The initiation of brittle faults in crystalline rock: Journal of Structural Geology, v. 77, p. 159-174, https://doi.org/10.1016/j.jsg.2015.05.001.

Eberhardt, E., Stimpson, B., and Stead, D., 1999, Effects of grain size on the initiation and propagation thresholds of stress-induced brittle fractures: Rock mechanics and rock engineering, v. 32, no. 2, p. 81-99.

Eichhubl, P., and Boles, J. R., 2000, Rates of fluid flow in fault systems; evidence for episodic rapid fluid flow in the Miocene Monterey Formation, coastal California: American Journal of Science, v. 300, no. 7, p. 571-600.

Ellis, D., Passey, S. R., Jolley, D. W., and Bell, B. R., Transfer zones: the application of new geological information from the Faroe Islands applied to the offshore exploration of intra and sub-basalt strata, *in* Faroe Islands Exploration Conference: Proceedings of the 2nd Conference, 2009, Annales Societatis Scientiarum Færoensis, p. 205-226.

Ellis, D., and Stoker, M. S., 2014, The Faroe–Shetland Basin: a regional perspective from the Paleocene to the present day and its relationship to the opening of the North Atlantic Ocean: Geological Society, London, Special Publications, v. 397, no. 1, p. 11-31.

Faulkner, D., Jackson, C., Lunn, R., Schlische, R., Shipton, Z., Wibberley, C., and Withjack, M., 2010, A review of recent developments concerning the structure, mechanics and fluid flow properties of fault zones: Journal of Structural Geology, v. 32, no. 11, p. 1557-1575.

Faulkner, D. R., Lewis, A. C., and Rutter, E. H., 2003, On the internal structure and mechanics of large strike-slip fault zones: field observations of the Carboneras fault in southeastern Spain: Tectonophysics, v. 367, no. 3, p. 235-251, https://doi.org/10.1016/S0040-1951(03)00134-3.

Faulkner, D. R., Sanchez-Roa, C., Boulton, C., and Hartog, S. A. M., 2018, Pore fluid pressure development in compacting fault gouge in theory, experiments, and nature: Journal of Geophysical Research: Solid Earth, v. 123, no. 1, p. 226-241.

Frery, E., Gratier, J.-P., Ellouz-Zimmerman, N., Loiselet, C., Braun, J., Deschamps, P., Blamart, D., Hamelin, B., and Swennen, R., 2015, Evolution of fault permeability during episodic fluid circulation: Evidence for the effects of fluid–rock interactions from travertine studies (Utah–USA): Tectonophysics, v. 651-652, p. 121-137, https://doi.org/10.1016/j.tecto.2015.03.018.

Frey, M., Capitani, C. d., and Liou, J., 1991, A new petrogenetic grid for low-grade metabasites: Journal of metamorphic Geology, v. 9, no. 4, p. 497-509.

Frolova, J., Ladygin, V., Rychagov, S., and Zukhubaya, D., 2014, Effects of hydrothermal alterations on physical and mechanical properties of rocks in the Kuril–Kamchatka island arc: Engineering Geology, v. 183, p. 80-95.

Gaina, C., Gernigon, L., and Ball, P., 2009, Palaeocene–Recent plate boundaries in the NE Atlantic and the formation of the Jan Mayen microcontinent: Journal of the Geological Society, v. 166, no. 4, p. 601, 10.1144/0016-76492008-112.

Gernigon, L., Gaina, C., Olesen, O., Ball, P., Péron-Pinvidic, G., and Yamasaki, T., 2012, The Norway Basin revisited: From continental breakup to spreading ridge extinction: Marine and Petroleum Geology, v. 35, no. 1, p. 1-19.

Gratier, J.-P., 2011, Fault Permeability and Strength Evolution Related to Fracturing and Healing Episodic Processes (Years to Millennia): the Role of Pressure Solution: Oil Gas Sci. Technol. – Rev. IFP Energies nouvelles, v. 66, no. 3, p. 491-506.

Gysi, A. P., and Stefánsson, A., 2012, Mineralogical aspects of CO2 sequestration during hydrothermal basalt alteration — An experimental study at 75 to 250°C and elevated pCO2: Chemical Geology, v. 306-307, p. 146-159, https://doi.org/10.1016/j.chemgeo.2012.03.006.

Hadizadeh, J., and Foit, F. F., 2000, Feasibility of estimating cementation rates in a brittle fault zone using Sr/Ca partition coefficients for sedimentary diagenesis: Journal of Structural Geology, v. 22, no. 4, p. 401-409, https://doi.org/10.1016/S0191-8141(99)00172-8.

Haines, S. H., Kaproth, B., Marone, C., Saffer, D., and van der Pluijm, B., 2013, Shear zones in clay-rich fault gouge: A laboratory study of fabric development and evolution: Journal of Structural Geology, v. 51, p. 206-225.

Hansen, H., Pedersen, A., Duncan, R., Bird, D., Brooks, C., Fawcett, J., Gittins, J., Gorton, M., and O'Day, P., 2002, Volcanic stratigraphy of the southern Prinsen af Wales Bjerge region, East Greenland: Geological Society, London, Special Publications, v. 197, no. 1, p. 183-218.

Hill, D. P., Reasenberg, P., Michael, A., Arabaz, W., Beroza, G., Brumbaugh, D., Brune, J., Castro, R., Davis, S., and dePolo, D., 1993, Seismicity remotely triggered by the magnitude 7.3 Landers, California, earthquake: Science, v. 260, no. 5114, p. 1617-1623.

Holland, M., Urai, J. L., and Martel, S., 2006, The internal structure of fault zones in basaltic sequences: Earth and Planetary Science Letters, v. 248, no. 1, p. 301-315, https://doi.org/10.1016/j.epsl.2006.05.035.

Ikari, M. J., Saffer, D. M., and Marone, C., 2009, Frictional and hydrologic properties of clay-rich fault gouge: Journal of Geophysical Research: Solid Earth, v. 114, no. B5.

Ivanova, I. I., and Knyazeva, E. E., 2013, Micro–mesoporous materials obtained by zeolite recrystallization: synthesis, characterization and catalytic applications: Chemical Society Reviews, v. 42, no. 9, p. 3671-3688.

Jébrak, M., 1997, Hydrothermal breccias in vein-type ore deposits: A review of mechanisms, morphology and size distribution: Ore Geology Reviews, v. 12, no. 3, p. 111-134, https://doi.org/10.1016/S0169-1368(97)00009-7.

Jørgensen, O., 2006, The regional distribution of zeolites in the basalts of the Faroe Islands and the significance of zeolites as palaeotemperature indicators: Geological Survey of Denmark and Greenland Bulletin, v. 9, p. 123-156.

Kettermann, M., Weismüller, C., von Hagke, C., Reicherter, K., and Urai, J. L., 2019, Large near-surface block rotations at normal faults of the Iceland rift: evolution of tectonic caves and dilatancy: Geology, v. 47, no. 8, p. 781-785.

Kington, J., 2013, mplstereonet: https://github.com/joferkington/mplstereonet, GitHub.
Kristmannsdóttir, H., 1979, Alteration of Basaltic Rocks by Hydrothermal-Activity at 100-300 °C, Developments in sedimentology, Volume 27, Elsevier, p. 359-367.
Larsen, L. M., Waagstein, R., Pedersen, A. K., and Storey, M., 1999, Trans-Atlantic correlation of the Palaeogene volcanic successions in the Faeroe Islands and East Greenland: Journal of the Geological Society, v. 156, no. 6, p. 1081-1095.
Larsen, R. B., and Tegner, C., 2006, Pressure conditions for the solidification of the Skaergaard intrusion: eruption of East Greenland flood basalts in less than 300,000 years: Lithos, v. 92, no. 1-2, p. 181-197.
Lee, Y.-J., and Morse, J. W., 1999, Calcite precipitation in synthetic veins: implications for the time and fluid volume necessary for vein filling: Chemical Geology, v. 156, no. 1, p. 151-170, https://doi.org/10.1016/S0009-2541(98)00183-1.
Logan, J., Experimental studies of simulated gouge and their application to studies of natural fault zones, *in* Proceedings of conference VIII: Analysis of Actual Fault zones in Bedrock, 1979, p. 305-343.
McKay, L., Lunn, R. J., Shipton, Z. K., Pytharouli, S., and Roberts, J. J., 2021, Do intraplate and plate boundary fault systems evolve in a similar way with repeated slip events?: Earth and Planetary Science Letters, v. 559, p. 116757, https://doi.org/10.1016/j.epsl.2021.116757.
Monzawa, N., and Otsuki, K., 2003, Comminution and fluidization of granular fault materials: implications for fault slip behavior: Tectonophysics, v. 367, no. 1, p. 127-143, https://doi.org/10.1016/S0040-1951(03)00133-1.
Moore, D. E., and Byerlee, J., 1992, Relationships between sliding behavior and internal geometry of laboratory fault zones and some creeping and locked strike-slip faults of California: Tectonophysics, v. 211, no. 1, p. 305-316, https://doi.org/10.1016/0040-1951(92)90067-G.
Morrow, C. A., Moore, D. E., and Lockner, D. A., 2017, Frictional strength of wet and dry montmorillonite: Journal of Geophysical Research: Solid Earth, v. 122, no. 5, p. 3392-3409, https://doi.org/10.1002/2016JB013658.
Neuhoff, P. S., Fridriksson, T., and Bird, D. K. J. I. G. R., 2000, Zeolite parageneses in the north Atlantic igneous province: Implications for geotectonics and groundwater quality of basaltic crust, v. 42, no. 1, p. 15-44.
Ólavsdóttir, J., Eidesgaard, Ó. R., and Stoker, M. S., 2017, The stratigraphy and structure of the Faroese continental margin: Geological Society, London, Special Publications, v. 447, no. 1, p. 339-356, 10.1144/sp447.4.
Otsuki, K., Monzawa, N., and Nagase, T., 2003, Fluidization and melting of fault gouge during seismic slip: Identification in the Nojima fault zone and implications for focal earthquake mechanisms: Journal of Geophysical Research: Solid Earth, v. 108, no. B4, https://doi.org/10.1029/2001JB001711.
Ougier-Simonin, A., and Zhu, W., 2015, Effect of pore pressure buildup on slowness of rupture propagation: Journal of Geophysical Research: Solid Earth, v. 120, no. 12, p. 7966-7985.
Passey, S., 2009, Recognition of a faulted basalt lava flow sequence through the correlation of stratigraphic marker units, Skopunarfjørður, Faroe Islands: Annales Societatis Scientiarum Færoensis, Tórshavn.
Passey, S. R., and Bell, B. R., 2007, Morphologies and emplacement mechanisms of the lava flows of the Faroe Islands Basalt Group, Faroe Islands, NE Atlantic Ocean: Bulletin of Volcanology, v. 70, no. 2, p. 139-156.
Passey, S. R., and Jolley, D. W., 2008, A revised lithostratigraphic nomenclature for the Palaeogene Faroe Islands Basalt group, NE Atlantic Ocean: Earth and Environmental Science Transactions of the Royal Society of Edinburgh, v. 99, no. 3-4, p. 127-158.
Peacock, D. C. P., 1991, Displacements and segment linkage in strike-slip fault zones: Journal of Structural Geology, v. 13, no. 9, p. 1025-1035, https://doi.org/10.1016/0191-8141(91)90054-M.
Peacock, D. C. P., and Sanderson, D. J., 1995, Strike-slip relay ramps: Journal of Structural Geology, v. 17, no. 10, p. 1351-1360, https://doi.org/10.1016/0191-8141(95)97303-W.
Proctor, B., Lockner, D., Kilgore, B., Mitchell, T., and Beeler, N., 2020, Direct evidence for fluid pressure, dilatancy, and compaction affecting slip in isolated faults: Geophysical Research Letters, v. 47, no. 16, p. e2019GL086767.
Renard, F., Beauprêtre, S., Voisin, C., Zigone, D., Candela, T., Dysthe, D. K., and Gratier, J.-P., 2012, Strength evolution of a reactive frictional interface is controlled by the dynamics of contacts and chemical effects: Earth and Planetary Science Letters, v. 341-344, p. 20-34, https://doi.org/10.1016/j.epsl.2012.04.048.
Renard, F., and Candela, T., 2017, Scaling of fault roughness and implications for earthquake mechanics: Fault Zone Dynamic Processes: Evolution of Fault Properties During Seismic Rupture, v. 227, p. 197-216.
Ritchie, J., and Hitchen, K., 1996, Early Paleogene offshore igneous activity to the northwest of the UK and its relationship to the North Atlantic Igneous Province: Geological Society, London, Special Publications, v. 101, no. 1, p. 63-78.
Roberts, N. M. W., and Walker, R. J., 2016, U-Pb geochronology of calcite-mineralized faults: Absolute timing of rift-related fault events on the northeast Atlantic margin: Geology, v. 44, no. 7, p. 531-534, 10.1130/g37868.1.
Rotevatn, A., Jackson, C. A. L., Tvedt, A. B. M., Bell, R. E., and Blækkan, I., 2019, How do normal faults grow?: Journal of Structural Geology, v. 125, p. 174-184, https://doi.org/10.1016/j.jsg.2018.08.005.
Roubeyrie, L., and Celles, S., 2018, Windrose: A Python Matplotlib, Numpy library to manage wind and pollution data, draw windrose: Journal of Open Source Software, v. 3, no. 29, p. 268.
Saffer, D. M., and Marone, C., 2003, Comparison of smectite- and illite-rich gouge frictional properties: application to the updip limit of the seismogenic zone along subduction megathrusts: Earth and Planetary Science Letters, v. 215, no. 1, p. 219-235, https://doi.org/10.1016/S0012-821X(03)00424-2.
Sagy, A., and Brodsky, E. E., 2009, Geometric and rheological asperities in an exposed fault zone: Journal of Geophysical Research: Solid Earth, v. 114, no. B2.
Sagy, A., Brodsky, E. E., and Axen, G. J., 2007, Evolution of fault-surface roughness with slip: Geology, v. 35, no. 3, p. 283-286, 10.1130/G23235A.1.
Seyfried, W. E., and Bischoff, J. L., 1979, Low temperature basalt alteration by sea water: an experimental study at 70°C and 150°C: Geochimica et Cosmochimica Acta, v. 43, no. 12, p. 1937-1947, https://doi.org/10.1016/0016-7037(79)90006-1.
Shimamoto, T., and Logan, J. M., 1981, Effects of simulated fault gouge on the sliding behavior of Tennessee sandstone: nonclay gouges: Journal of Geophysical Research: Solid Earth, v. 86, no. B4, p. 2902-2914.
Shipton, Z. K., Soden, A. M., Kirkpatrick, J. D., Bright, A. M., and Lunn, R. J., 2006, How thick is a fault? Fault displacement-thickness scaling revisited.
Sibson, R. H., 1990, Conditions for fault-valve behaviour: Geological Society, London, Special Publications, v. 54, no. 1, p. 15-28.

Sleep, N. H., and Blanpied, M. L., 1992, Creep, compaction and the weak rheology of major faults: Nature, v. 359, no. 6397, p. 687-692, 10.1038/359687a0.
Soden, A. M., and Shipton, Z. K., 2013, Dilational fault zone architecture in a welded ignimbrite: The importance of mechanical stratigraphy: Journal of Structural Geology, v. 51, p. 156-166, https://doi.org/10.1016/j.jsg.2013.02.001.
Stel, H., 1981, Crystal growth in cataclasites: diagnostic microstructures and implications: Tectonophysics, v. 78, no. 1-4, p. 585-600.
Storey, M., Duncan, R. A., and Tegner, C., 2007, Timing and duration of volcanism in the North Atlantic Igneous Province: Implications for geodynamics and links to the Iceland hotspot: Chemical Geology, v. 241, no. 3, p. 264-281, https://doi.org/10.1016/j.chemgeo.2007.01.016.
Sutherland, R., Toy, V. G., Townend, J., Cox, S. C., Eccles, J. D., Faulkner, D. R., Prior, D. J., Norris, R. J., Mariani, E., Boulton, C., Carpenter, B. M., Menzies, C. D., Little, T. A., Hasting, M., De Pascale, G. P., Langridge, R. M., Scott, H. R., Lindroos, Z. R., Fleming, B., and Kopf, A. J., 2012, Drilling reveals fluid control on architecture and rupture of the Alpine fault, New Zealand: Geology, v. 40, no. 12, p. 1143-1146, 10.1130/G33614.1.
Tembe, S., Lockner, D. A., and Wong, T. F., 2010, Effect of clay content and mineralogy on frictional sliding behavior of simulated gouges: Binary and ternary mixtures of quartz, illite, and montmorillonite: Journal of Geophysical Research: Solid Earth, v. 115, no. B3.
Utada, M., 2001, Zeolites in burial diagenesis and low-grade metamorphic rocks: Reviews in mineralogy and geochemistry, v. 45, no. 1, p. 277-304.
Virgo, S., Abe, S., and Urai, J. L., 2013, Extension fracture propagation in rocks with veins: Insight into the crack-seal process using Discrete Element Method modeling: Journal of Geophysical Research: Solid Earth, v. 118, no. 10, p. 5236-5251.
Von Hagke, C., Kettermann, M., Bitsch, N., Bücken, D., Weismüller, C., and Urai, J. L., 2019, The effect of obliquity of slip in normal faults on distribution of open fractures: Frontiers in Earth Science, v. 7, p. 18.
Waagstein, R., Guise, P., and Rex, D. J. G. S., London, Special Publications, 2002, K/Ar and 39Ar/40Ar whole-rock dating of zeolite facies metamorphosed flood basalts: the upper Paleocene basalts of the Faroe Islands, NE Atlantic, v. 197, no. 1, p. 219-252.
Waagstein, R., Hald, N., Jørgensen, O., Nielsen, P. H., Noe, A., Jørgensen, O., Noe-nygaard, A., and Schonharting, G., 1984, Deep drilling on the Faeroe Islands.
Walker, R. J., Holdsworth, R. E., Armitage, P. J., and Faulkner, D. R., 2013a, Fault zone permeability structure evolution in basalts: Geology, v. 41, no. 1, p. 59-62, 10.1130/G33508.1.
Walker, R. J., Holdsworth, R. E., Imber, J., and Ellis, D., 2011, Onshore evidence for progressive changes in rifting directions during continental break-up in the NE Atlantic: Journal of the Geological Society, v. 168, no. 1, p. 27-48.
Walker, R. J., Holdsworth, R. E., Imber, J., and Ellis, D., 2012, Fault-zone evolution in layered basalt sequences: A case study from the Faroe Islands, NE Atlantic margin: GSA Bulletin, v. 124, no. 7-8, p. 1382-1393, 10.1130/B30512.1.
Walker, R. J., Holdsworth, R. E., Imber, J., Faulkner, D. R., and Armitage, P. J., 2013b, Fault zone architecture and fluid flow in interlayered basaltic volcaniclastic-crystalline sequences: Journal of Structural Geology, v. 51, p. 92-104, https://doi.org/10.1016/j.jsg.2013.03.004.
Walsh, J., Bailey, W., Childs, C., Nicol, A., and Bonson, C., 2003, Formation of segmented normal faults: a 3-D perspective: Journal of Structural Geology, v. 25, no. 8, p. 1251-1262.
Warren-Smith, E., Fry, B., Wallace, L., Chon, E., Henrys, S., Sheehan, A., Mochizuki, K., Schwartz, S., Webb, S., and Lebedev, S., 2019, Episodic stress and fluid pressure cycling in subducting oceanic crust during slow slip: Nature Geoscience, v. 12, no. 6, p. 475-481.
Wästeby, N., Skelton, A., Tollefsen, E., Andrén, M., Stockmann, G., Claesson Liljedahl, L., Sturkell, E., and Mörth, M., 2014, Hydrochemical monitoring, petrological observation, and geochemical modeling of fault healing after an earthquake: Journal of Geophysical Research: Solid Earth, v. 119, no. 7, p. 5727-5740.
Weismüller, C., Urai, J. L., Kettermann, M., Hagke, C. v., and Reicherter, K., 2019, Structure of massively dilatant faults in Iceland: lessons learned from high-resolution unmanned aerial vehicle data: Solid Earth, v. 10, no. 5, p. 1757-1784.
Wibberley, C. A. J., Yielding, G., and Di Toro, G., 2008, Recent advances in the understanding of fault zone internal structure: a review: Geological Society, London, Special Publications, v. 299, no. 1, p. 5, 10.1144/SP299.2.
Williams, R. T., 2019, Coseismic boiling cannot seal faults: Implications for the seismic cycle: Geology, v. 47, no. 5, p. 461-464.
Woodcock, N. H., and Mort, K., 2008, Classification of fault breccias and related fault rocks: Geological Magazine, v. 145, no. 3, p. 435-440, 10.1017/S0016756808004883.
Yukselen-Aksoy, Y., 2010, Characterization of two natural zeolites for geotechnical and geoenvironmental applications: Applied Clay Science, v. 50, no. 1, p. 130-136.

9 Figures

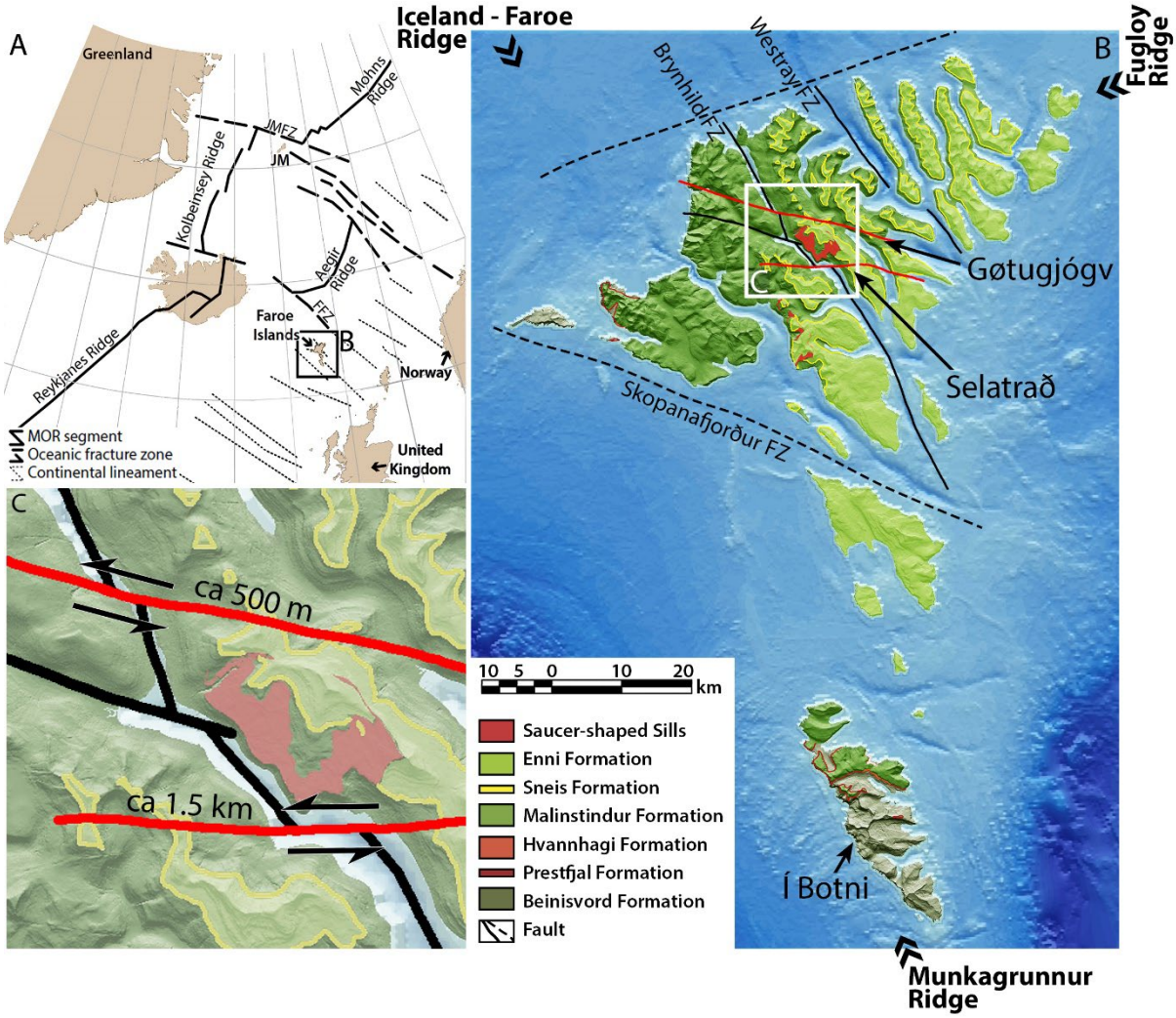

Figure 1: Structural overview and geological setting of the Faroe Islands. (A) The archipelago in the N-Atlantic sits on the intersection of three ocean ridges: the Iceland-Faroe Ridge in the NW, the Fugloy Ridge in the NE and the Munkagrunnur Ridge in the S (after Roberts and Walker, 2016). (B) We focus on three fault zones in this paper: Two large sinistral strike-slip faults exposed in Gøtugjógv and Selatrað (Eysturoy), and a smaller normal fault exposed in Í Botni (Suðuroy). (C) The fjord separating Eysturoy (E) from Streymoy (W) indicates the position of the major Brynhild fault zone (FZ), which is offset by the Gøtugjógv and Selatrað fault zones, indicating potential displacements of 500 m and 1.5 km respectively.

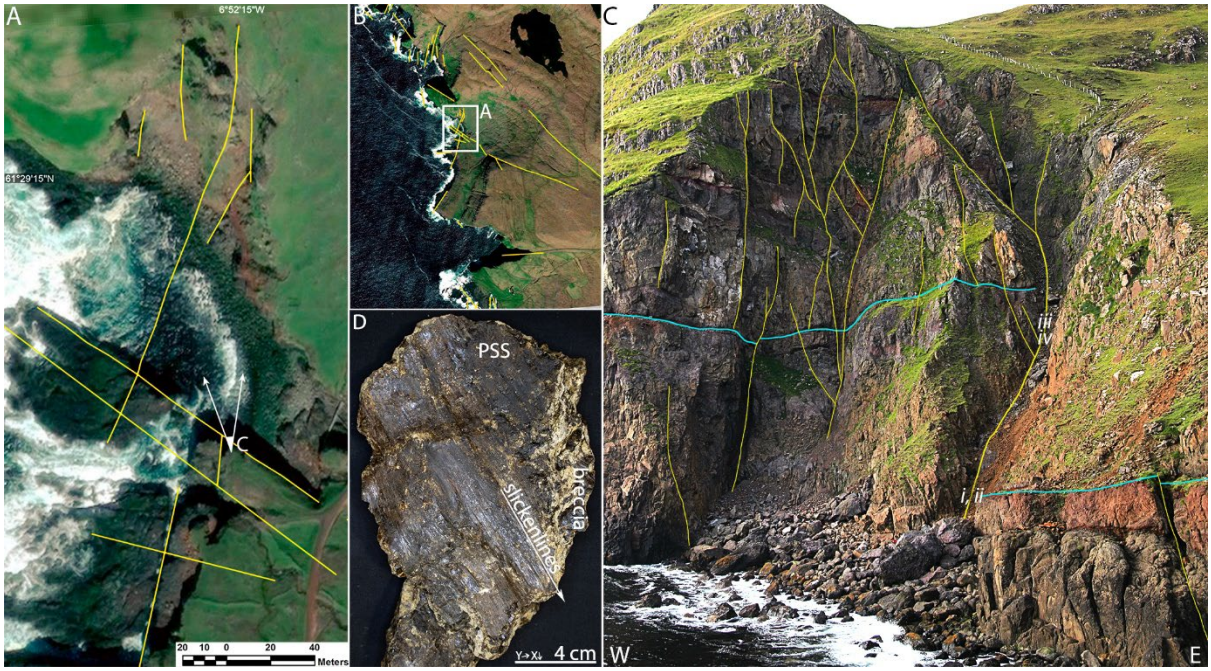

Figure 2: The Í Botni fault zone (61°29'14"N, 6°52'18"W) is a 50 m wide and very steep fault zone with an E-down sense of movement. Only the main fault strand concentrating essentially all of the 30 m displacement in the E was sampled (i – iv, Figure 8 - Figure 10). It has an average orientation of 280/69° with striations on a highly polished slip surface (D: sample IBO-i) plunging 303/82°.

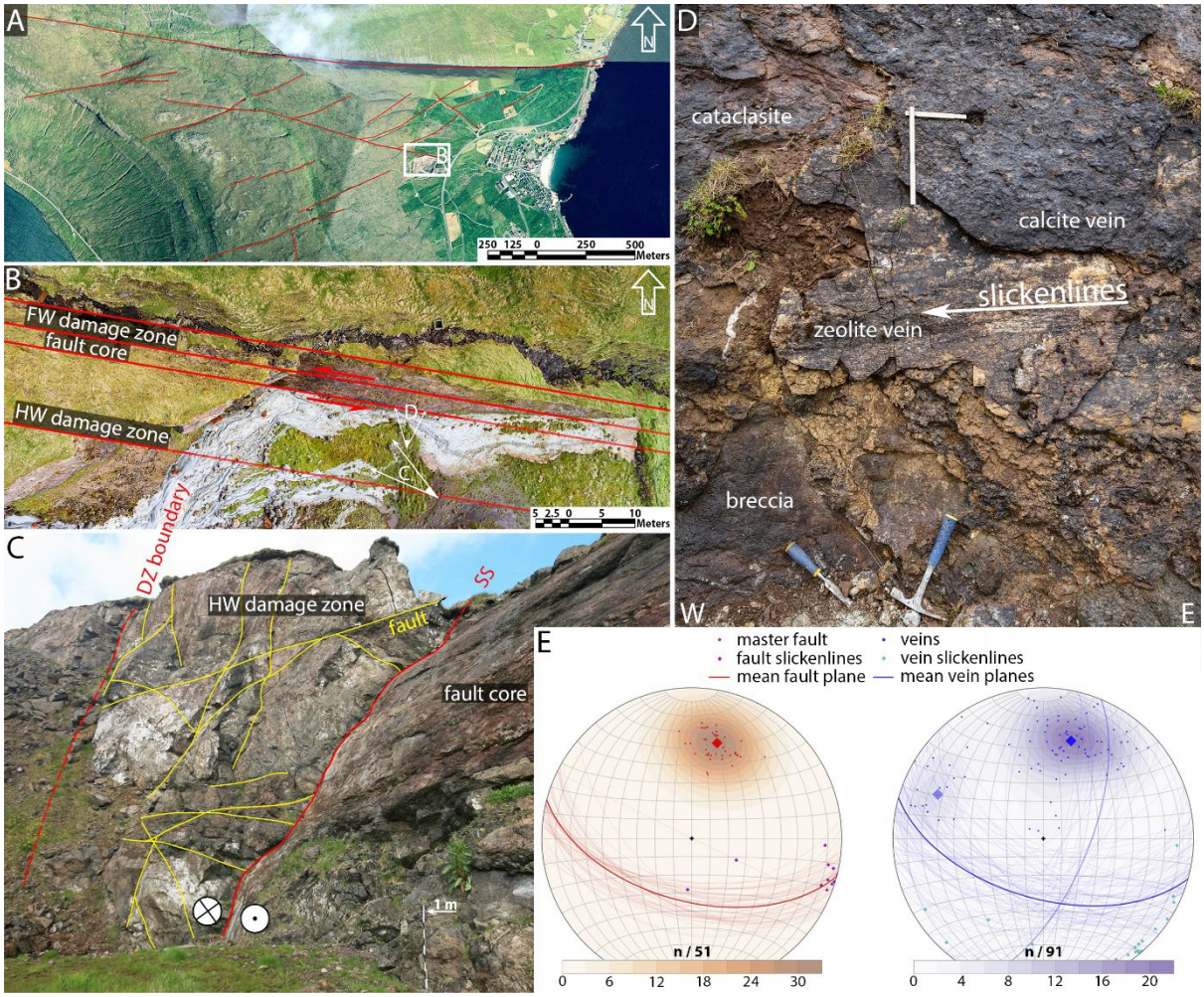

Figure 3: (A) The sinistral fault zone in Gøtugjógv (62°11'11"N, 6°45'47"W) is surrounded by a wide array of small Riedel faults. (B) A diagonal transect from the hanging wall damage zone in the W to the footwall damage zone in the E is exposed in a disused quarry. The exposed footwall section, containing most of the fault core is 50 m wide and up to 10 m high. (B & C) The exposed section is distinctly asymmetrical. The damage zone is 10 m wide in the hanging wall as opposed to only 3 m in the footwall. The fault core, however, is mainly contained in the footwall, with a width of 2–3 m vs 20–30 cm in the hanging wall. (C) The slip surface (SS) is strongly corrugated, exposing 3–4 marked asperities. The ruler for scale is 1 m long. (D) Large patch of fault parallel veins exploiting the contact between two cataclasite lenses in the slip zone. The contact between the zeolite and calcite vein is smooth and heavily striated by sinistral slickenlines. Average orientation of slickenlines on the slip surface and veins is 104/08°. Ruler is 40 x 20 cm. (E) Average slip surface orientation (red) is rather shallow for a strike-slip fault with 194/56° and shows little scatter. The fault core hosts extensive veining (blue), predominantly parallel (74/91 veins) or orthogonal (17/91 veins) to the slip surface.

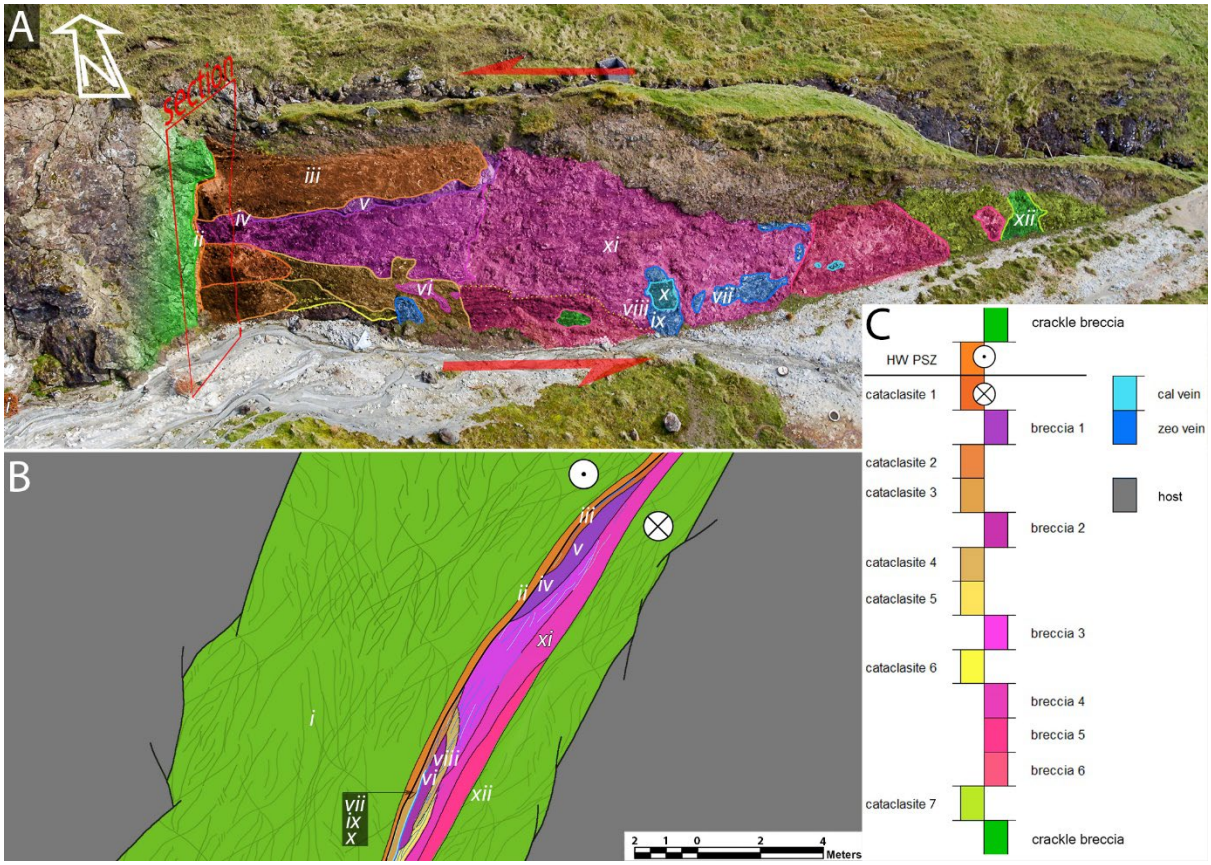

Figure 4: Fault rock distribution in the Gøtugjógv fault zone (A) in the field and (B, legend in C) in a stylised section. The damage zone is mainly composed of a coarse crackle breccia with unaltered host rock clasts. This is contrasted by the highly altered and reworked fault core material which is composed of lenticular fault rock bodies separated by cataclastic shear bands and/or veins. Close to the principal slip zone, these fault rock lenses mostly contain cataclasite. Closer to the damage zone breccias become more prevalent. They are almost exclusively the result of hydrofracture and are cemented by zeolite or calcite with a texture similar to vein cements. Indices i – xii refer to samples and micrographs in Figure 8 and Figure 10.

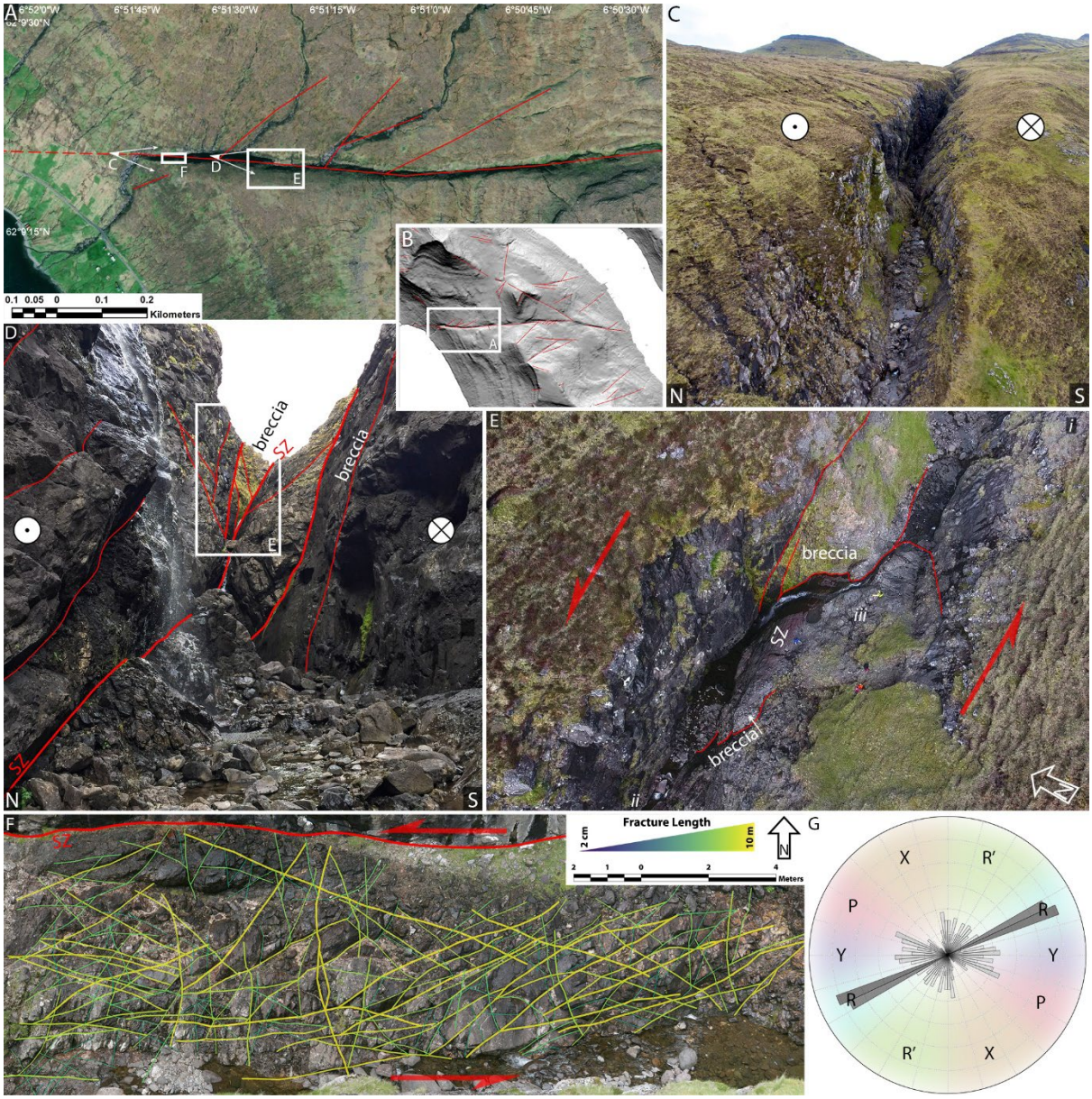

Figure 5: The sinistral Selatrað fault zone can be traced across (B) the entire southwestern peninsula of Eysturoy, but is only exposed in two deep gorges on either coast. We focus on the western gorge (A & C, 62° 9'19"N, 6°51'25"W). Smaller faults (in red) in the wider area follow Riedel orientation in (A) the direct vicinity but (B) are less organised further away. (D) The overall topographic orientation of the gorge is 000/60° and is presumed to be indicative of fault zone orientation. Slip zone (SZ) and secondary faults mostly run parallel to this trend with a mean orientation of 000/71°. (D & E) The slip zone meanders through the fault zone, switching from (E) its southern edge on the upper tier exposed in the west (D) to the northern edge further down. The slip zone and secondary faults bound lenses of fragmented older fault rock. (F & G) Internal fracturing in these lenses is highly systematic and follows the typical Riedel orientation with a very strong dominance of R shears. Indices i – iii in panel E are locations of samples shown in Figure 9. PSS—principal slip surface.

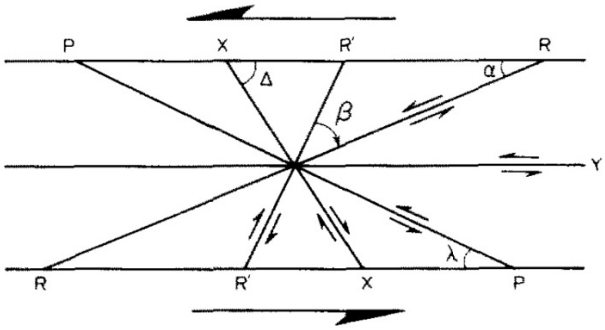

Figure 6: Riedel shear (P, X, R', R, Y) configuration developed in simple shear (Logan, 1979).

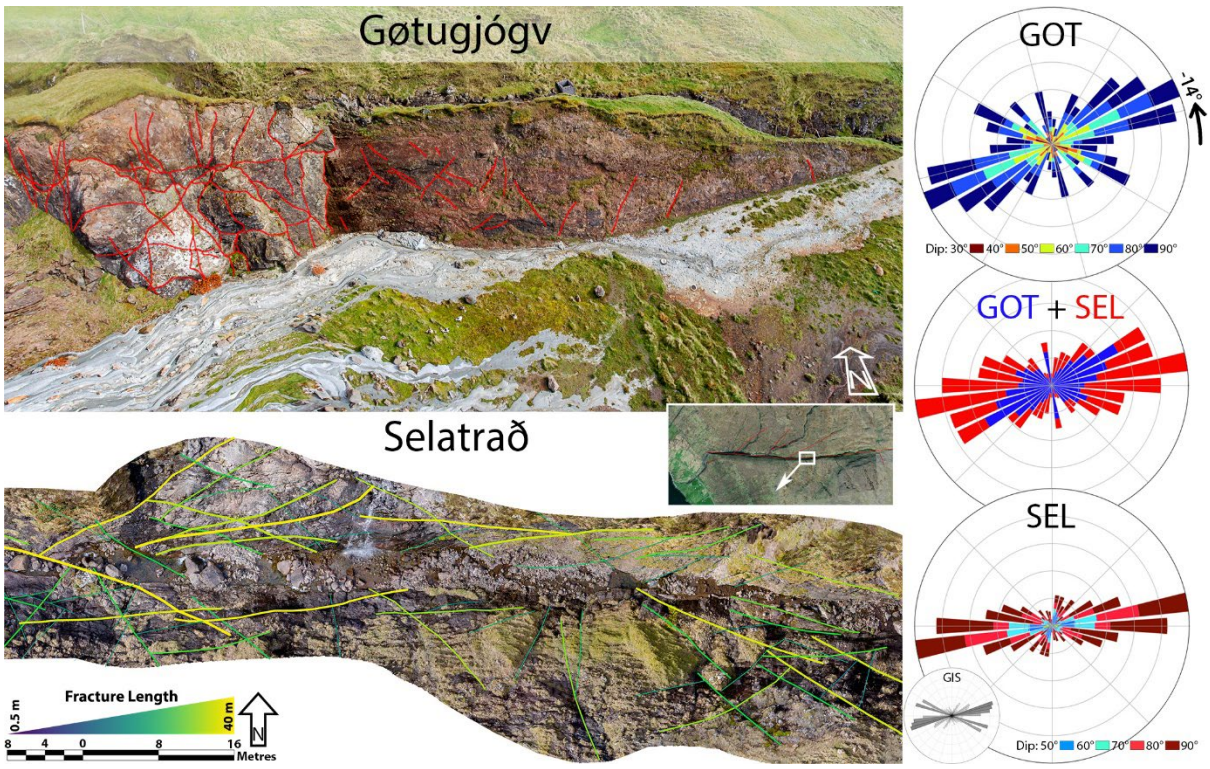

Figure 7: Comparison between secondary fault orientation in Gøtugjógv and Selatrað. The Gøtugjógv rose plot was rotated 14° anticlockwise to match the E-W trend of Selatrað. The data plotted were measured in the field and on fault planes interpreted in the virtual outcrop models. They were given equal weight, i.e. half of the data are the field measurements, and the other half are virtual outcrop measurements. The pictures do not represent the plotted data but are rather examples of the general look of the fault zones. The Gøtugjógv data show a more balanced distribution between R, P, R' and X shears. Y shears are essentially absent because measurements from the slip surface were excluded. The Selatrað data are strongly dominated by Y and R shears, most likely because these are very prominent in the gorge, introducing a bias in the field measurements. This becomes clear when comparing to the lineament analysis performed in GIS (inset rose plot), which confirms R frequency recorded in the field and virtual outcrop, but also has a similarly strong peak around the P orientation. In any case, we can see similar trends in both fault zones. R (and Y) shears are the dominant orientation with subordinate P shears and much less common high angle R' and X shears. Also see Figure 5F & G for smaller scale structures.

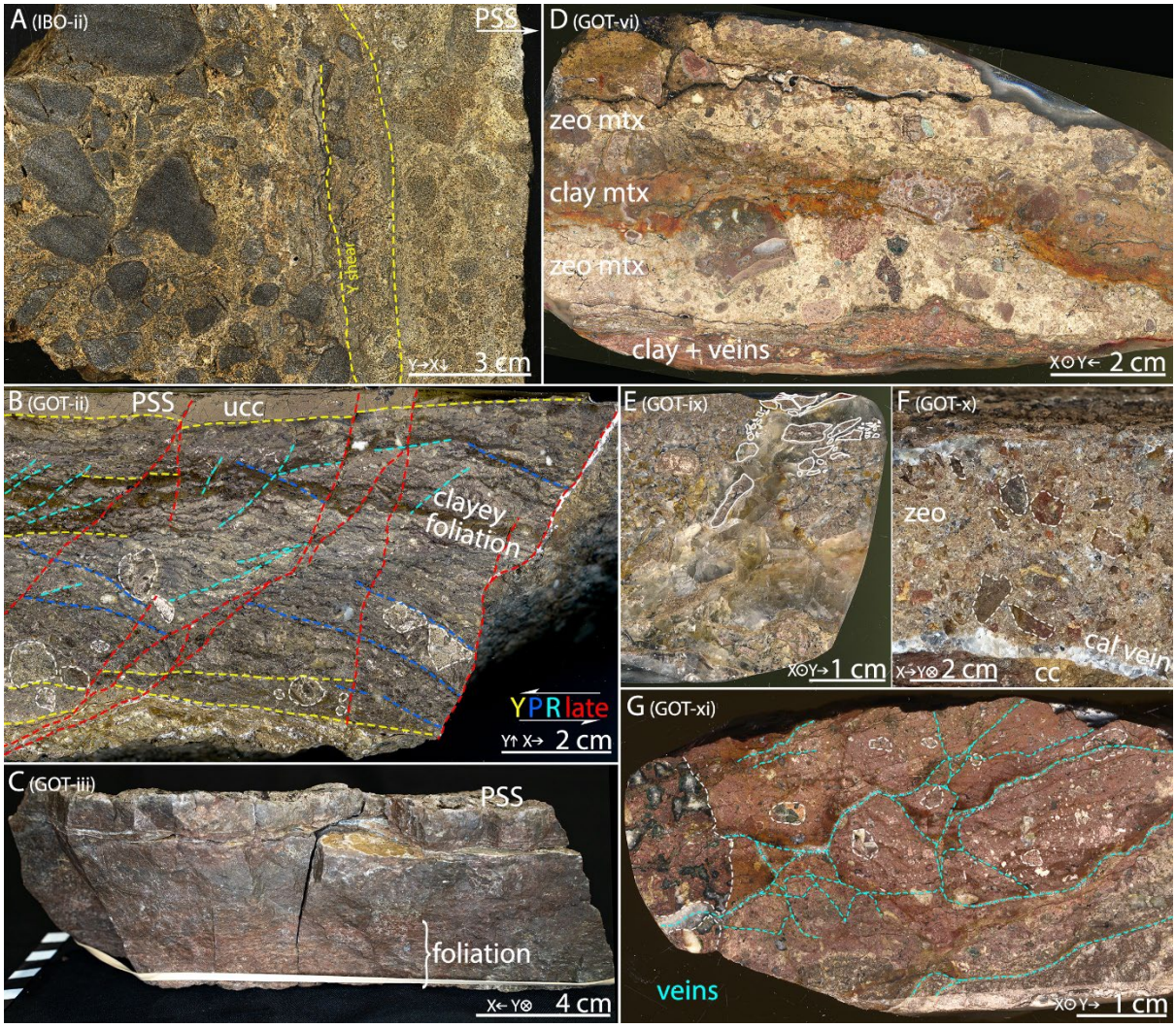

Figure 8: Specimen scale structure of fault rocks: (A) Transition from a coarse chaotic breccia to finer breccia and protocataclasite a few centimetres away from the principle slip surface (PSS) in Í Botni. (B) The hanging wall slip zone (sinistral in picture) in Gøtugjógv is defined by a thin layer of ultracataclasite (ucc) separated by Y shears (yellow) from a 5 cm thick cataclasite with a clayey foliation along P (blue) and R (teal) shears. Both the foliation and the contact are transected by late-stage high angle shears (red). (C) The footwall slip surface, on the other hand, is a >5 cm thick layer of homogeneous ultracataclasite with a very weak foliation on the far side, which is not distinguishable in thin sections. The boundary cutting across the sample parallel to the slip surface is a tabular zeolite-calcite vein. (D) Chaotic breccia of generally fine grained (<5 mm) clayey fault rock clasts in a zeolite or zeolite + clay matrix (zeo/clay mtx). (E & F) Hydrofractured, chaotic breccia with fault rock clasts (outlined in white) in € coarse, equant calcite or (F) fine acicular-bladed zeolite cement (F). (G) Red (ultra-) cataclasite hydrofractured into a crackle breccia with thin zeolite veins. Exemplary clasts are outlined in white.

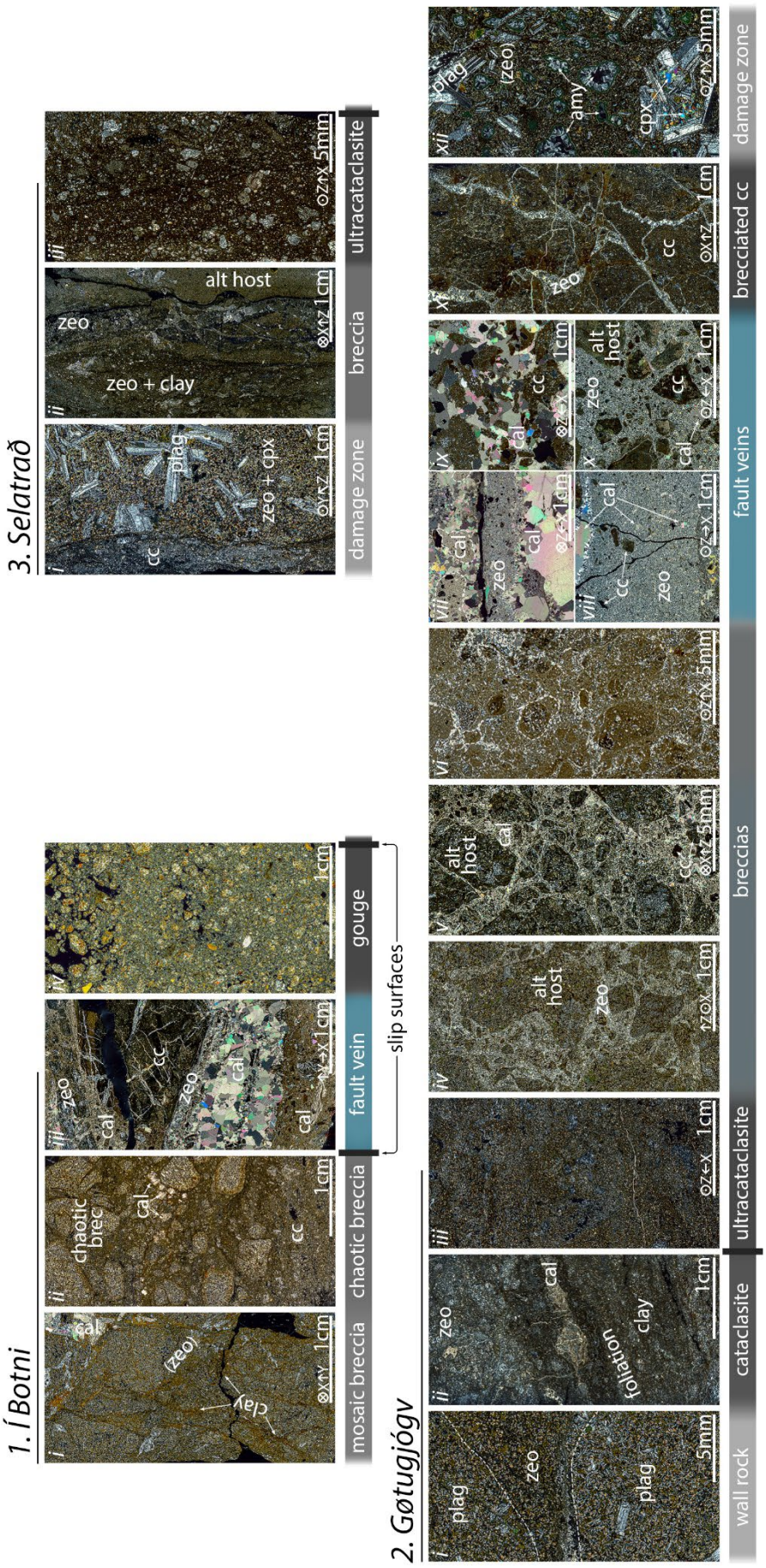

Figure 9: Microstructures as found along fault transects. 1. In the low displacement Í Botni (IBO) fault zone, slip surfaces separate mosaic (i) and chaotic (ii) breccias with partially altered matrix from a slip zone with strongly altered and cemented breccia (iii) as well as unconsolidated gouge (iv). 2. Gøtugjógv (i) hanging wall damage zone with fractures delimiting an area of zeolitised host in otherwise unaltered host. (ii) Foliated hanging wall cataclasite from the slip zone with both clay and zeolite dominated matrix as opposed to (iii) thick homogeneous ultracataclasite in the foot wall. The footwall fault core contains lenses of chaotic breccia with altered host clasts in deformed zeolite (iv) or calcite (v) cement, as well as (vi) reworked fault rock clasts and substantially more clay in the zeolitic cement. The fault core is also the site of significant veining (vii – x). Especially thick veins commonly host variable concentrations of wall rock fragments (ix & x) but can also reactivate and rework older veins (vii). Their contacts are striated, and deformation is accommodated in a thin shear layer along the boundary (bottom of viii). (xi) Older cataclasite is reworked into a crackle breccia by irregular hydrofracture veins close to (xii) the essentially unaltered (minor matrix zeolitisation) porphyritic damage zone basalt in the footwall. 3. Selatrað features highly altered and localised secondary faults in an otherwise weakly altered damage zone (i + right side of ii), similar to GOT-xii. The slip zone is characterised by a homogeneous (ultra-) cataclasite with a clay dominated matrix. Abbreviations: alt—altered, amy—amygdale, brec—breccia, cal—calcite, cc—cataclasite, plag—plagioclase, ucc—ultracataclasite, zeo—zeolite. See Figure 10 for textural details. All micrographs in cross-polarised light.

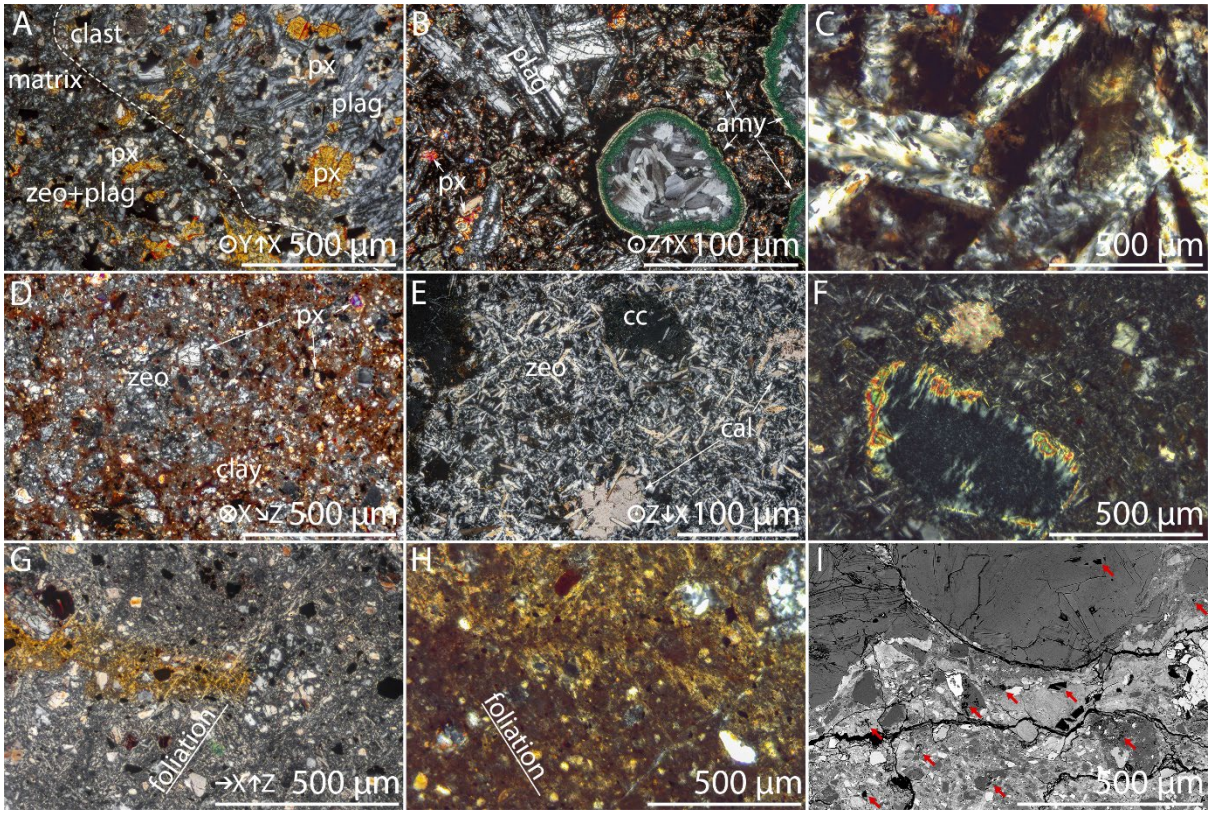

Figure 10: Photomicrographs of textural details: (A – IBO-ii) Í Botni slip zone chaotic breccia with yet unaltered plagioclase in the clasts and partially zeolitised cataclastic matrix. (B – GTO-xii) Gøtugjógv footwall damage zone of relatively unaltered porphyritic basalt clast with zeolite filled amygdales and plagioclase phenocrysts in partially altered groundmass. (C – GOT-iv) Botryoidal zeolite replacing plagioclase in a Gøtugjógv breccia clast. (D – GOT-iii) Homogeneous footwall ultracataclasite from the Gøtugjógv slip surface. Shape preferred orientation of zeolite crystals in veins (E – GOT-viii) and cataclasite matrix (F – GOT-ii) from Gøtugjógv. Also note the euhedral zeolite crystals growing into the calcite pocket in E. Foliation in zeolite (G – GOT-iii) and clay dominated (H – GOT-ii) slip surface ultracataclasite, Gøtugjógv. (I – GOT-ii) Porosity in slip zone cataclasite from Gøtugjógv in SEM-BSE. Abbreviations: amy—amygdale, cal—calcite, cc—cataclasit, plag—plagioclase, px—pyroxene, zeo—zeolite. All micrographs except in panel I are in cross-polarised light.

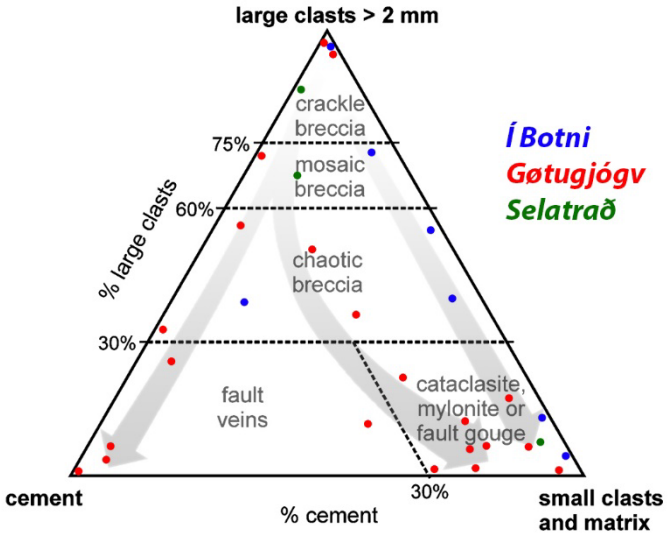

Figure 11: Plotting samples from all three fault zones in the fault rock classification diagrams by Woodcock and Mort (2008) shows that fault rock evolution roughly follows three trends: In the first phase of fault growth (Í Botni, blue), fault rocks are composed almost exclusively of host rock clasts and comminuted matrix. In more mature faults (Gøtugjógv, red & Selatrað, green), the fault rocks range either on a spectrum of cemented breccias spanning from crackle breccia to veins, or diverge from this trend by accumulating fine grained matrix through cataclasis of clasts and cement from initial brecciation.

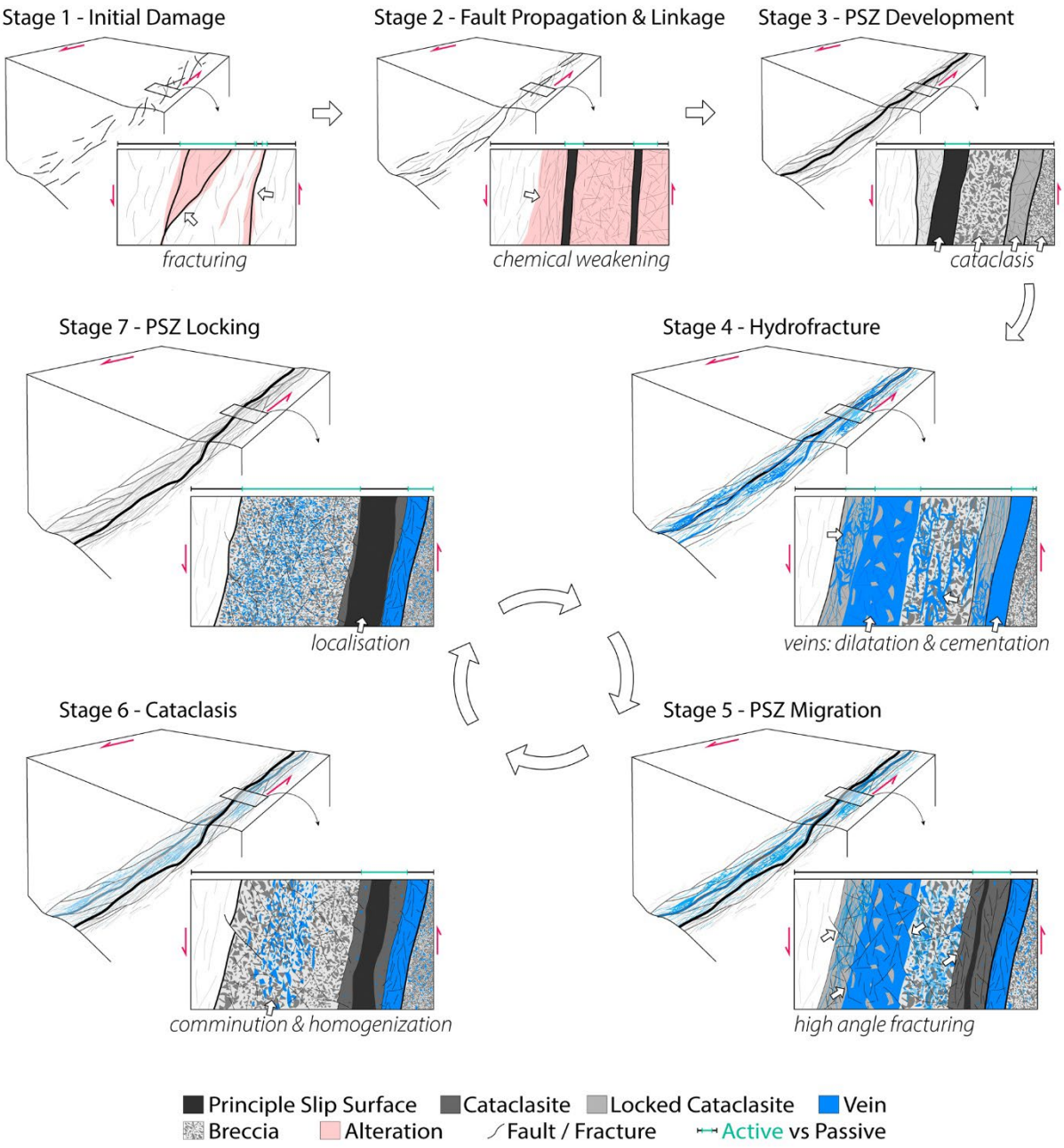

Figure 12: Simplified conceptual fault zone evolution in basaltic rock. (Stage 1, GOT-i) Initial distributed damage leads to channelling of fluid flow and associated alteration and weakening of wall rock. (Stage 2, IBO-i - iii) Fault strands linkage followed by slip localisation into cataclastic principal slip zone (PSZ) increases permeability, initiating fluid-mediated alteration of fault rocks. (Stage 3, GOT-iii & SEL-i) Pervasive fault rock alteration leads to weakening and further slip localisation and cataclasis. (Stage 4, GOT-ix – xi) Progressive comminution and increasing clay concentration reduce PSZ permeability, culminating in fluid overpressure, hydrofracture, and mineralisation/cementation. (Stage 5, GOT-xi) The now strengthened PSZ is abandoned, and slip migrates to a weaker part of the fault zone. (Stage 6, GOT-v & vi) The abandoned fault rock is reworked by cataclasis in the vicinity of the newly localised slip zone and integrated into second generation breccia and cataclasite. (Stage 7) Similar to stage 3, cataclasis and alteration in the new PSZ, again, lead to a permeability drop, closing the cycle. (Second entry in parentheses refers to micrographs representing the respective stages in Figure 9.)

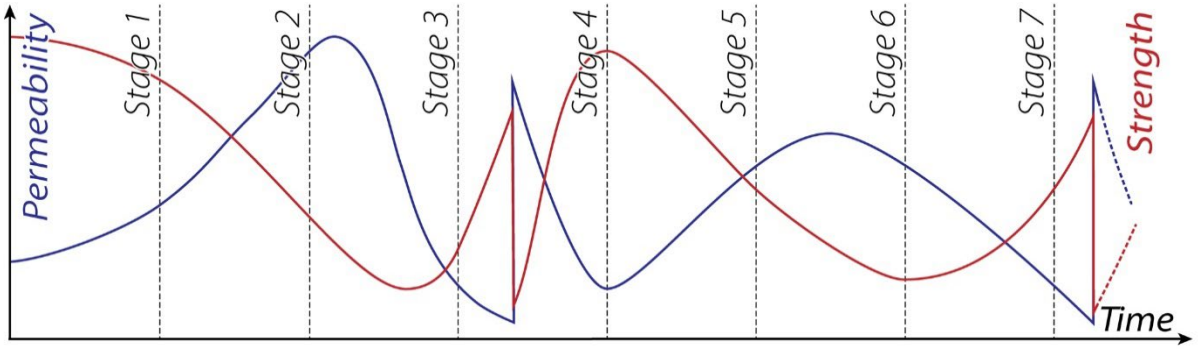

Figure 13: Hypothesised fault-parallel permeability (blue) and strength evolution (red). Stages from Figure 12. Initial fracturing enhances permeability while strength is reduced (stages 1-2). Once a cataclastic slip zone is established, grain comminution and increasing clay concentration through alteration reduce permeability and lead to strain-hardening (stage 3), until eventually overpressurised trapped fluids trigger hydrofracture. Cementation restrengthens the core and closes fluid pathways, quickly reducing permeability (stage 4). Reworking in the newly formed slip zone breaks up the cements, reducing strength, and initially increasing permeability (stages 5-6), until the reduced grain size, again, leads to strain-hardening and permeability loss (stage 7).